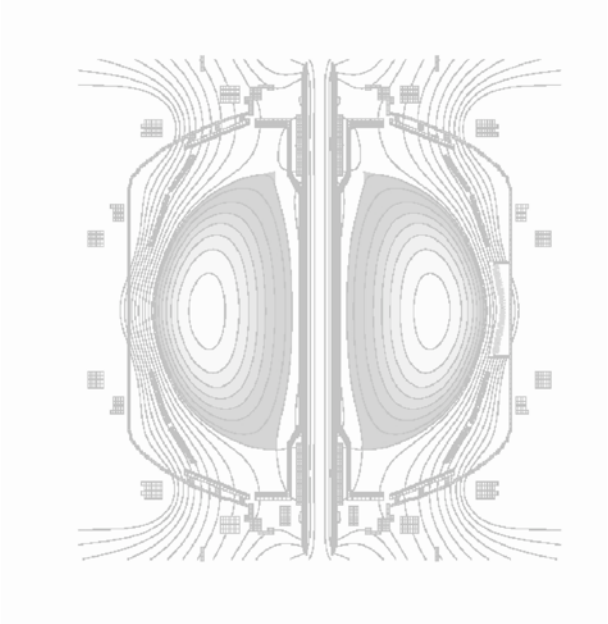

Chapter 2

The NSTX National Fusion Facility - Status and Upgrades

The National Spherical Torus Experiment (NSTX) at the Princeton Plasma Physics Laboratory (PPPL) is a proof-of-principle facility built to carry out research on the spherical torus (ST) plasma configuration. The NSTX research mission is to evaluate the physics principles of the ST, which is characterized by strong magnetic field curvature and high β_T, the ratio of the plasma pressure to the applied toroidal magnetic field pressure. This provides a fertile ground for cutting-edge plasma research. The programmatic mission of NSTX is to determine, through the scientific investigation, the attractiveness of the ST for developing practical fusion energy systems. Operational since 1999, the NSTX has been steadily building up its facility and diagnostic capabilities.

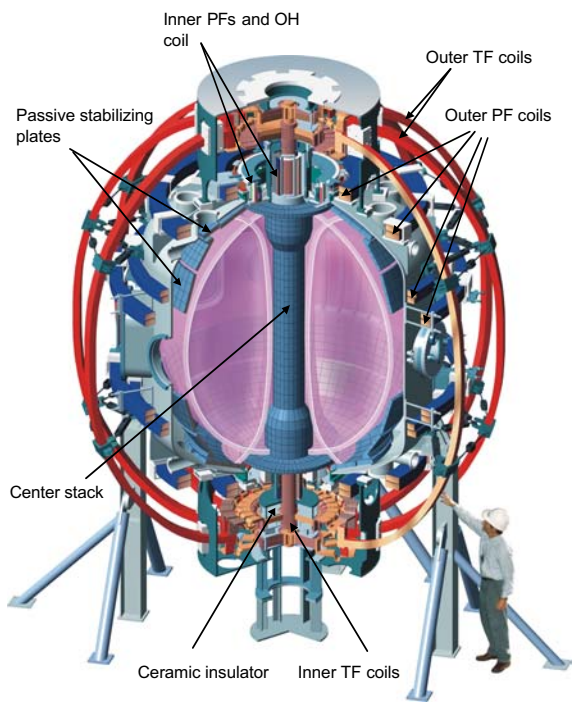

Fig. 2.1. NSTX Device Schematic

Achieved Parameters	
Aspect ratio	1.27
Elongation	2.2
Triangularity	0.8
Plasma Current	1.5 MA
Toroidal Field	0.6T
Heating and Current Drive:	
Induction	0.7Vs
NBI	7MW
HHFW	6MW
CHI	0.4MA
Pulse Length	1.1s
Gas fueling	LFS + HFS

Table 2.1. Achieved Facility Parameters

2.1 Achievements and Status

NSTX is a major component of the restructured U.S. Fusion Energy Sciences Program, which emphasizes the investigation of innovative confinement concepts and the advancement of the underlying physics to strengthen the scientific basis for attractive fusion power. To accomplish this mission, the NSTX facility (Figure 2.1) was designed with the following capabilities:

- Low aspect ratio, $R/a \geq 1.26$, and shaped plasma cross-section with nominal elongation $\kappa \approx 2.0$ and triangularity $\delta \approx 0.6$;
- Plasma current I_p up to 1 MA and toroidal magnetic field B_{T0} up to 0.6 T (at the nominal major radius, 0.85 m);
- Inductive solenoid and Coaxial Helicity Injection (CHI) for startup to 0.5 MA;
- High Harmonic Fast Wave system (6 MW), Neutral Beam Injection (5 MW) and CHI for heating, current drive, and current profile control;

- Close-fitting conducting plates to maximize MHD stability at high plasma pressure;
- Toroidal field pulse length (at 0.3 T) up to 5 s >> skin time ~ 0.3 s.

2.1.1 Progress in Facility Capabilities

As can be seen in Table 2.1, the NSTX facility has already achieved or exceeded many of its original design capabilities. In particular, the plasma current, a key parameter for plasma performance, reached 1.5 MA, 50 % over the original design value of 1 MA. In Fig. 2.2, we show the plasma current progress with calendar time. The figure also shows the introduction date for some relevant facility capabilities which contributed to the progress.

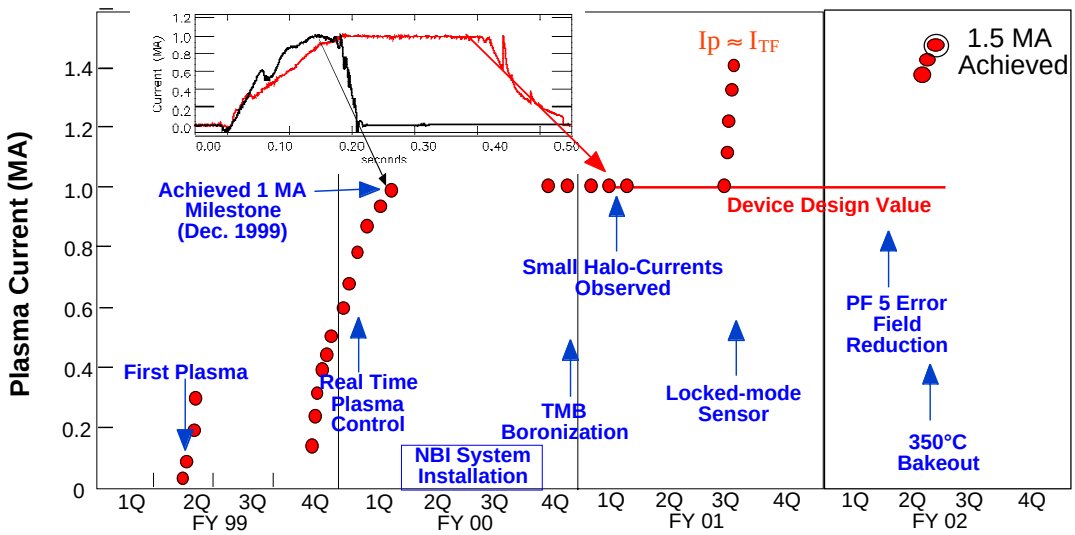

Fig. 2.2. Progress in the maximum NSTX plasma current with time.

Initial Shake-Down and Operation – As shown in Fig. 2.2, the NSTX facility began operation in February 1999, about three months ahead of schedule. By December 1999, NSTX reached its design plasma current of 1 MA, about nine months ahead of schedule. This rapid progress to 1 MA was made possible by the reliable power supply system available from TFTR and by the early implementation of the real-time plasma control system to control the plasma radial and vertical position and the plasma current. The ORNL electron cyclotron heating preionization (ECH-P) system also proved to be helpful in achieving rapid plasma initiation. In this period of operation, all of the basic plasma shapes specified in the NSTX physics requirements were produced in ohmically heated plasmas. In September 2000, NBI heating was brought in to operation. This, together with the introduction of boronization of the plasma facing surfaces, improved the plasma performance markedly. The inset figure compares the first 1 MA

discharge with one obtained about a year later. The overall discharge duration increased by a factor 2.5 to 0.5 s while the current flat-top time increased from essentially zero to about 200 ms.

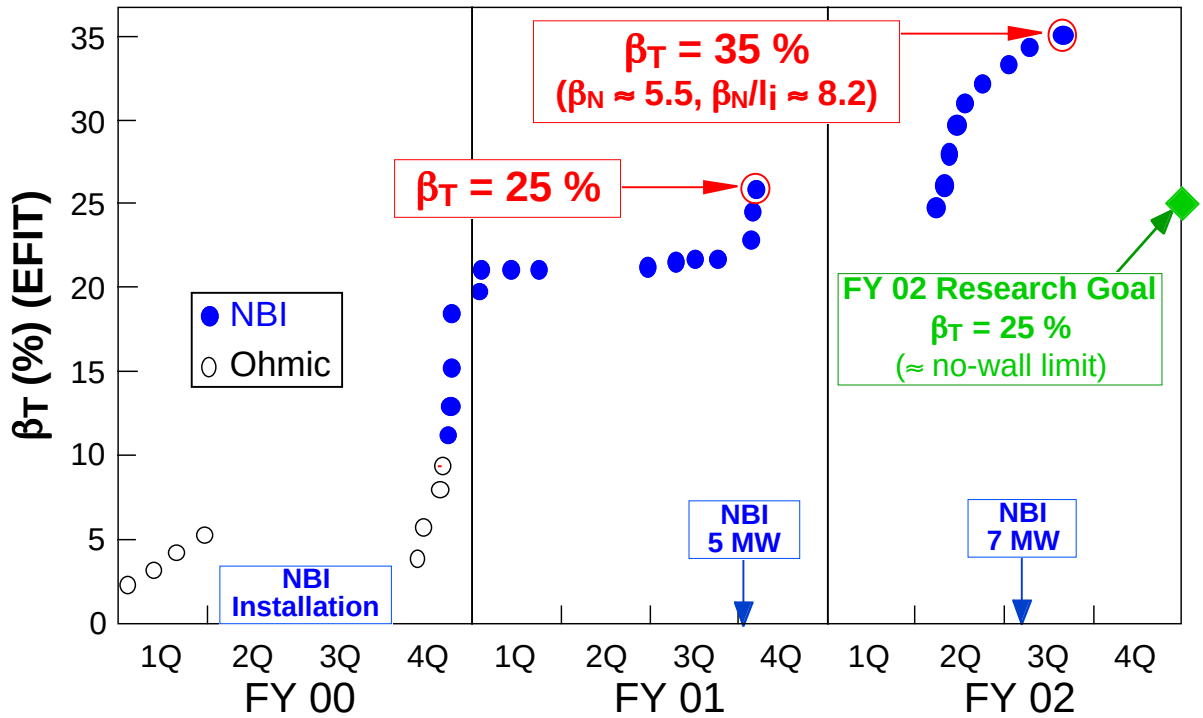

Fig. 2.3. Progress of average toroidal beta with time.

Increased Plasma Current and NBI Heating Capabilities – With the introduction of neutral beam injection (NBI), the NSTX research emphasis moved to investigating the strongly heated discharge regime. Figure 2.3 shows the rapid progress achieved in the average toroidal beta, β_T (= $2\mu_0\langle p\rangle/B_{T0}^2$, where $\langle p\rangle$ is the volume-average total plasma kinetic pressure and B_{T0} is the vacuum toroidal field at the plasma geometric center). An important element for maximizing β_T is the plasma current capability. During the experiments in early FY 01, the resistive flux consumption gradually decreased due to the combined effects of reduced impurities, achieved through boronization, and higher plasma temperature produced by the NBI heating. Analysis showed that it should be possible to achieve higher plasma current without increasing the stresses on the coils or the vacuum vessel, so, after an engineering review, the decision was made to increase the allowable plasma current to 1.5 MA. From the device safety point of view, this decision was based, among other considerations, on the relatively benign behavior of the wall halo-current measured during disruptions in both NSTX and the MAST device at the UKAEA Culham Laboratory. With the increased plasma current limit, NSTX made rapid progress and reached 1.5 MA in June 2001.

Further progress in plasma performance was aided by facility improvements, including the 350°C high-pressure-helium bakeout system and the realignment of the outermost poloidal-field (PF5) coils to minimize the error fields. This realignment reduced the amplitude of the n = 1 component of the radial field at the plasma edge by about a factor of 12, to less than 0.2 mT, *i.e.* $<10^{-3}B_P$, under typical discharge conditions, and reduced the occurrence of locked MHD modes which had developed in earlier high-current plasmas. It should be noted that with this high plasma current, NSTX reached another significant milestone of ST performance, namely where the plasma current equals or exceeds the toroidal field current through the center conductor bundle. Maximizing the ratio of the plasma current to the toroidal field current is an important objective for ST research to improve the viability of the ST for a fusion power plant.

The NBI system also continued to progress and in April 2002, after engineering review, the NBI power was increased to 7 MW at an accelerating voltage of 100 kV, significantly above the design value of 5 MW at 80 kV. This produced the highest plasma stored energy yet in NSTX, 390 kJ, and widened the overlap of the NSTX operating regime with that of conventional tokamaks for studying the influence of aspect ratio on toroidal plasma confinement and transport.

Progress in Confinement and β – During 2002, boronization, helium glow discharge cleaning and high-current helium discharges were applied to reduce gas recycling and impurity influx from the wall. This promoted the formation of the edge transport barrier characteristic of the H-mode in conventional tokamaks. The plasma energy confinement time reached about 1.5 times the value projected for NSTX parameters from the ITER H-mode database developed from tokamak experiments. It is interesting to note that the highest plasma global confinement time in NSTX of over 100 ms has been achieved *with* NBI heating, whereas confinement times of about 30 ms are typically obtained in ohmic discharges. In addition to its effects on confinement, the H-mode produces broad plasma pressure profiles favorable for high β stability. As a result, the plasma toroidal beta reached the FY 02 goal of $\beta_T = 25\%$ more than one year ahead of schedule. Then, in March 2002, the H-Mode phase was extended to essentially the full duration of the programmed period of constant plasma current. Finally, the plasma toroidal beta reached 35% at $I_p = 1.2$ MA in June 2002.

Development of Plasma Control – Plasma control is a central element of advanced ST research. The capabilities of the NSTX plasma control system have been improving steadily. As a result, discharges with very high triangularity, $\delta \approx 0.8$, well above the original design value of 0.6, have been produced, as shown in Fig. 2.4. These high triangularity plasmas are the highest performing discharges in NSTX in plasma toroidal beta and stored energy.

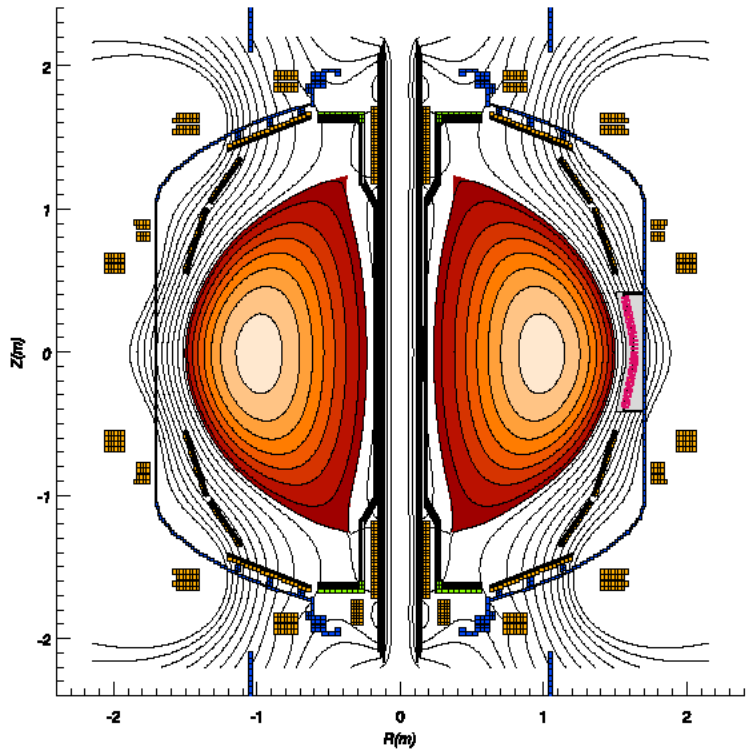

Fig. 2.4. Flux contours from EFIT analysis of a highly shaped ($\delta \approx 0.8$, $\kappa \approx 2.2$) high-performance ($\beta_T = 35\%$) plasma.

In June 2002, control of the plasma was demonstrated with the plasma equilibrium calculated every 10 ms by the real-time EFIT (rt-EFIT) code. This control, which was implemented successfully on NSTX as a joint effort with General Atomics, represents an important milestone toward developing the versatile plasma control system needed to achieve the advanced ST operational goals. The application of rt-EFIT was extended in the 2003 run. Several of the basic plasma shapes were run under rt-EFIT control, including double-null divertor plasmas in which the X-point, outer gap and triangularity were simultaneously controlled using all the PF coils. Basic discharge templates for several standard plasma conditions were created for use in subsequent experiments.

Experiments on High Harmonic Fast Wave Heating – The high plasma beta and dielectric constant of ST plasmas make the wave accessibility particularly challenging for heating the plasma by RF waves using conventional schemes. However, High Harmonic Fast Waves (HHFW) are expected to be able to heat electrons in an ST to high temperatures and to contribute to sustaining the plasma current. Modeling calculations suggest good accessibility and power absorption of HHFW for typical NSTX plasmas. A twelve-element-antenna system, shown in Fig. 2.5, was designed and installed by PPPL and ORNL as a

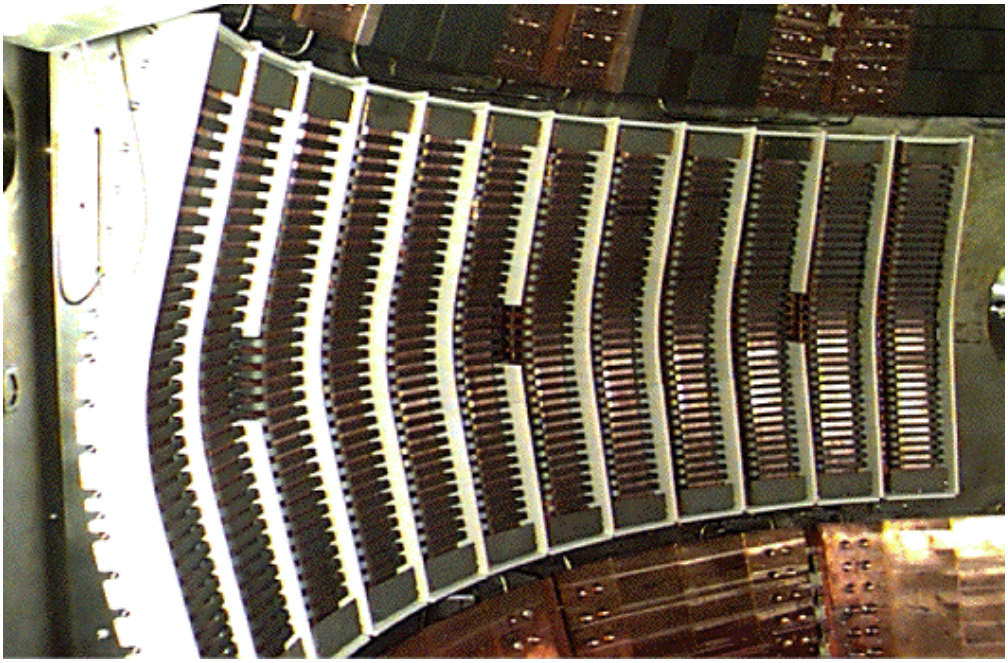

Fig. 2.5. 12-Element HHFW Antenna System in the NSTX Vacuum Vessel.

joint project with the Enabling Technology Program of the DOE Office of Fusion Energy Sciences. Pairs of antenna elements are driven by six RF power amplifiers operating at 30 MHz with independent control of the phase of the RF current in the six pairs. The phase control system is designed to vary the parallel wave-number $k_{\parallel}$ of the launched waves from 14 m^{-1} to about 4 m^{-1} in real time, to follow the discharge evolution from low-temperature, start-up plasmas to high-temperature, high-beta plasmas. This corresponds to changing the parallel phase velocity of the waves from 1.3×10^7 m/s to 4.7×10^7 m/s to match the typical electron thermal velocity for $T_e = 1 – 10$ keV.

Strong electron heating by HHFW was observed for the first time in NSTX experiments. The electron temperature was increased from about 0.4 keV to about 4 keV using 3 MW of HHFW power. Experiments to study HHFW current drive have demonstrated a significant change in the loop voltage as the direction of the driven current was varied, consistent with the theoretical expectations.

The HHFW system has delivered 6 MW into the plasma. However, above about 3 MW, the system reliability has been hampered by arcing in the antenna feedthroughs. The feedthrough area was modified during the FY 02 outage to improve its voltage stand-off capability, which resulted in improving the antenna power handling capability by 50% from about 3.5 MW to 5 MW during the brief FY 03 run. This suggests that the power handling capability of the antenna could be further improved by implementing a double end-fed, center-ground design, which would increase its coupled power by a factor of four for the same feed-through voltage. (See Sec. 3.3.)

Progress on Coaxial Helicity Injection – For an attractive ST power plant, the OH solenoid must be eliminated in the center stack. Although this represents a major departure from conventional tokamak designs, the relatively modest magnetic flux and helicity per unit plasma current for ST tend to ease non-inductive startup requirements. The technique for non-inductive startup tested to date in NSTX is coaxial helicity injection (CHI). The method has been investigated previously in smaller devices including HIT/HIT-II (U. Washington) and HIST (Himeji Institute, Japan). However, the NSTX experiment represents a significant step in terms of plasma volume and magnetic flux from the HIT-II experiment as shown in Table 2.2.

Machine	R (m)	a (m)	B_T (T)	Toroidal Flux (mWb)	I_{inj} (kA)	V_{inj} (kV)	I_{tor} (kA)	Multiplier	Pulse Length (ms)
HIT-II	0.3	0.2	0.5	50	30	0.5	200	7	20
NSTX	0.86	0.68	0.3	500	28	0.6	400	14	400

Table 2.2. Comparison of CHI systems on NSTX and HIT-II

A schematic of CHI is shown in Fig. 2.6 (a). Ceramic insulating rings, located at the top and bottom of the device, electrically insulate the center-stack from the outer vacuum vessel, allowing a potential difference to be applied. With the appropriate gas fill pressure (typically in the few mTorr range) and with a voltage of up to 1 kV applied, a plasma discharge can be initiated between the inner and outer divertor plates. Using the lower PF coils, a stronger poloidal field is applied at the bottom gap, reducing the connection length there, so that the discharge is initiated preferentially across it. The applied toroidal field

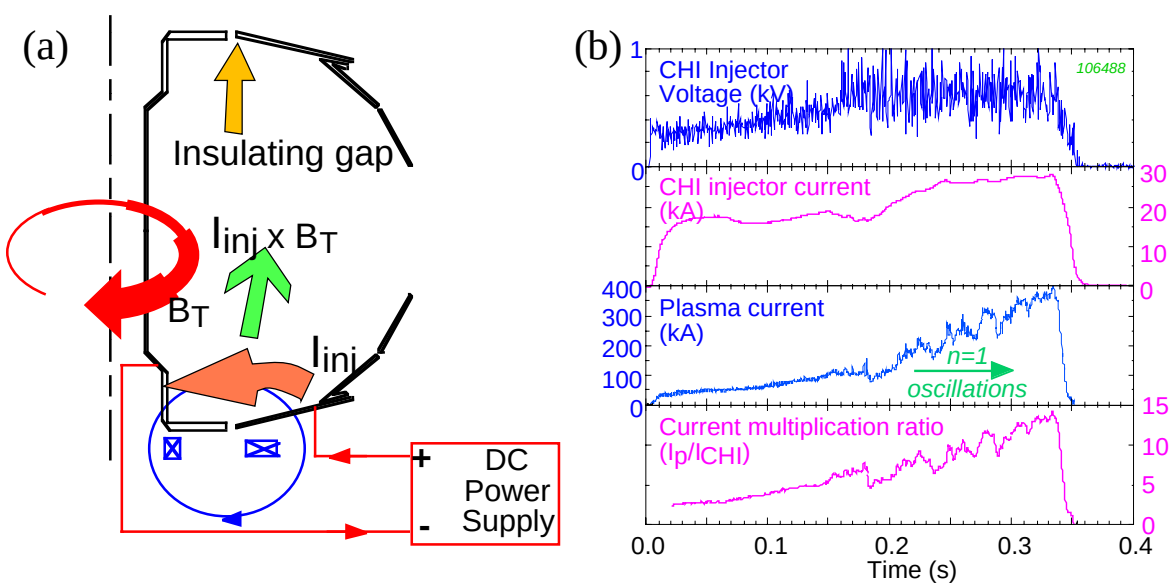

Fig. 2.6 (a). Schematic of CHI configuration. *(b) CHI discharge evolution.*

causes the current in the plasma to develop a strong toroidal component, the beginning of the desired toroidal plasma current. If the injector current exceeds a threshold value, the resulting ΔB_{tor}^2 or $\mathbf{J}_{pol} \times \mathbf{B}_{tor}$ stress across the current layer exceeds the field-line tension of the injector flux causing plasma in the lower divertor region, and its associated helicity, to move into the main chamber. In Fig. 2.6 (b), CHI discharge waveforms are shown in which the toroidal current is driven from zero without the solenoid. Toward the end of the 300 ms discharge, a toroidal current of 390 kA has been generated with only about 28 kA of injected current, a current amplification factor of ~14. This represents an excellent efficiency. What remains to be demonstrated is the transfer of the driven toroidal current from flowing on open field lines connecting the electrodes to closed magnetic surfaces through the process of magnetic reconnection, and then the coupling of the CHI-produced plasma to other means of non-inductive current sustainment. Recent experiments on the HIT-II device have demonstrated the successful transfer of a CHI-induced plasma to inductive ramp-up with a substantial saving of poloidal flux. Experiments to develop this method, known as "transient CHI", were initiated in NSTX early in 2003.

As the current was increased in the early CHI experiments in NSTX, the discharges were frequently terminated by arcs across the insulating gap at the top (termed the absorber gap). When such arcing occurs, the vacuum vessel forms a low impedance electrical path which short-circuits the injector and terminates the helicity injection. To suppress the arcs, a new insulator for the absorber gap was designed and fabricated in FY 02. This insulator creates a much longer path for an arc to bridge the absorber gap and the indications from the FY 03 run are that the new design is indeed more resistant to arcing.

Boundary Physics and Related Facility Developments – The achievement of good vacuum and surface conditions on the plasma-facing components (PFCs) has been crucial to the progress in plasma performance in NSTX. The nominal plasma-facing area is 41 m^2; about 75% (31 m^3) consists of graphite (or carbon-fiber composite in some high heat-flux areas) tiles on areas close to the plasma boundary and the remaining 25% is the vessel wall (304 stainless steel), well away from the plasma surface. The mass of the carbon PFCs is 1.3×10^3 kg. High temperature bake-out is used to expedite the removal of water and CO absorbed in the near-surface regions. In FY 03, the upgraded bake-out system was used to perform a uniform bake-out of the carbon PFCs to 350 C for the first time. The inner PFCs on the center-stack are heated resistively by passing current through the inner inconel tube of the vacuum vessel while the outer PFCs are heated by circulating high-pressure helium through internal tubes.

After bakeout and again after about every two weeks of plasma operation, boronization is applied to the plasma facing surfaces by running a glow discharge, usually in a mixture of deuterated trimethylboron (TMB, $(CD_3)_3B$) gas (10% by volume) in helium, although pure TMB gas has also been used with similar results. In addition, daily helium glow discharge cleaning (HeGDC) and inter-discharge HeGDC are also used for impurity and density control during high-power operation. This combination of vacuum surface preparation methods suppresses oxygen impurities. In addition, the discharge-averaged hydrogen to

deuterium ratio for plasmas with deuterium gas fueling decreased from above 0.2 immediately following a major vacuum opening to below 0.05 after bake-out followed by boronization, and continued decreasing. Experiments exploring the potential for real-time deposition of boron films by injecting small quantities of TMB into the plasma edge have shown promise. The wall conditioning effort to date has facilitated many of the advances made in the NSTX research program. The plan for NSTX includes upgrades designed to improve impurity control, fueling efficiency, profile and particle control.

2.1.2 TF Fault and TF Bundle Repair Work

On Feb. 14, 2003, after four weeks of FY 03 plasma operation, the toroidal field (TF) coil developed an electrical fault during a shot and failed. Fig. 2.7(a) shows the coil current waveforms for the pulse which failed (red) and the preceding normal pulse (blue). The current trace showed no anomalies prior to the fault. The coil fault detection system shut down the power supply immediately after detecting the fault condition. The failure occurred at a lower joint between one of the inner-leg (axial) conductors and its radial "flag" at the location shown in Fig. 2.7(b). The flag, that was bolted to the conductor in the inner bundle to create a current carrying joint, separated from the inner conductor and moved radially outward by about one inch creating a gap at the joint. A photograph of the failed joint is shown in Fig. 2.7(c). An arc was created across the gap, that was sustained by the inductive energy stored in the coil itself, damaging the surrounding area and necessitating the replacement of the TF center bundle. Fortunately, because the TF power supply shut down rapidly and the support structure formed a protective barrier, there was no significant collateral damage to the neighboring structures, which include the OH and PF coils, vacuum vessel, and diagnostics. The TF bundle was taken out of the machine approximately one week after the failure without breaking high vacuum, so it was possible to perform calibrations of diagnostics afterwards to validate data taken during the FY 03 run.

After the FY 02 operation period when the toroidal field was used at its full design value of 0.6 T, the joints had been examined and many, particularly those in the lower half, were found to be out of specification. The lower joints, including the failed joint, were therefore refurbished and all their resistances were brought back within the established specification. Before the FY 03 run started, a decision was made to limit the toroidal field to 0.45 T. A program was instituted to examine a rotating fraction of the joints during every maintenance period, *i.e.,* each 2 – 3 weeks of operation, whereas previously, the joints had been examined annually. The resistances of the upper joints were measured and the torques on the flag bolts were checked during the Feb. 3 maintenance week after three weeks of operation. Although all the resistances were satisfactory, some bolts of the more highly stressed flags, in the tier nearer the midplane, had fallen below their specified torque. The lower joints, including the one that failed, were scheduled to be examined during the maintenance week scheduled to start on Feb. 24 but, unfortunately, the failure occurred before this.

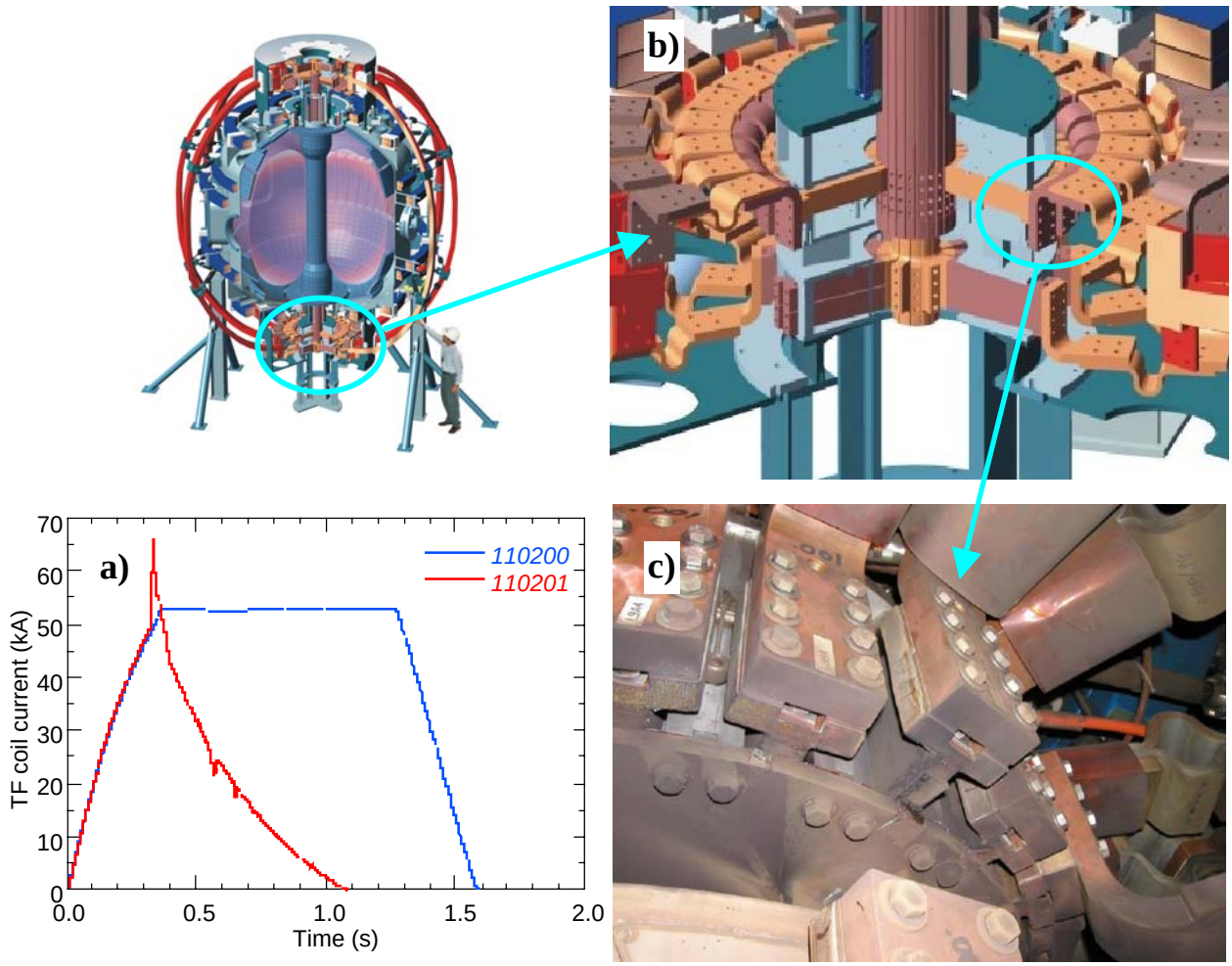

Fig.2.7 (a) TF coil current for the failed pulse (red) and the preceding normal pulse (blue);
(b) Schematic of the lower joint region where the fault occurred;
(c) Photo of the separated TF joint: the flag assembly is displaced outward by about 1"

Following the failure, the design basis for the flag joint and hub structure was reanalyzed. It was found that the stiffness of the hub, which reacts the axial load on the flags, had been overestimated by the original finite element analysis due to an assumption that the flag and hub could not slide with respect to one another. As a result the flag fasteners were under-designed. The reanalysis showed that the structure was adequate for the initial operation at 0.3 T, and even at 0.45 T, but not at 0.6 T. Even though a limited number of 0.6 T shots were executed, they led to the deterioration and eventual failure of a joint during a less stressful 0.45 T pulse.

A concerted design and R&D effort was launched to develop a new joint. After extensive analysis and modelling with finite-element structure codes, a design was developed that satisfies the stringent mechanical and electrical requirements. A design review for the TF joint engineering was held at PPPL on April 10, 2003. The review team included external reviewers from General Atomics, MIT, Culham Laboratory (UK) and the University of Wisconsin. Many valuable recommendations were generated, including performing additional analyses for variations of friction coefficients and thermal conditions, using higher strength bolts, improving the shear key design, additional component testing particularly with cyclical loads at elevated temperatures, and improved joint instrumentation. The project will hold another review to verify that all of the issues have been addressed. The effect of fatigue on the joints will be tested by subjecting prototypes to up to 50,000 cycles, which is equivalent to more than 10 years of operation with high facility utilization.

Since manufacturing defects had been discovered in the original TF inner bundle, the copper conductor for a new bundle had been purchased in FY 01. This copper stock is a long lead item, so that decision was fortunate. As result, the fabrication of the replacement TF bundle is proceeding relatively rapidly now that the redesign of the joints and their supporting structure has been finalized. The schedule calls for resuming plasma operation in Feb. 2004, allowing sufficient time in FY 04 to carry out the planned 21-run-week schedule.

With this new TF coil, the facility reliability should improve to accommodate the significant increase in plasma operation time to about 21 run weeks per year upon which progress in this Five-Year Plan is based. With the improved joint design, the time associated with joint maintenance can presumably be reduced The new joint is designed for routine operation of the TF up to the original specifications.

2.1.3 Facility Utilization

The NSTX facility utilization is shown in Table 2.3. As shown in the table, except in FY 03, the NSTX facility operated according to the planned run weeks. The facility reliability has steadily improved throughout the period. In FY 02, the operation actually exceeded the planned 12 run weeks and also achieved 90% plasma availability. Due to the relatively mature state of the NSTX facility, the number of run weeks as we move forward is mainly determined by budget availability. The utilization of the NSTX facility in FY 02 by researchers, post-doctoral researchers and students is also shown in Table 2.3.

Facility Availability for Plasma Operation

	FY 00	FY 01	FY 02	FY 03	FY 04-08
Run weeks planned	15	15	12	12	21
Run weeks achieved	15	15	13	4	
Hours of operation	600	600	520	160	840

Participating Research Personnel in FY 03

	PPPL	non-PPPL
Research Staff	45	85*
Post Doc.	3	7
Grad. Students	5	5
Undergrad. Students	3	5

* Including 15 collaborating researchers from foreign institutions in countries including Japan, Russia, Korea, UK, Ukraine, and Canada.

Table 2.3: Facility Utilization

2.1.4 Progress in Plasma Diagnostics

The plasma diagnostic set on NSTX has been steadily expanding and improving, despite a very constrained budget for diagnostic upgrades. The programmatic priority in this initial phase of operations has been implementing diagnostics to measure the basic plasma properties. The major diagnostics currently installed and operating are listed in Table 2.4 below. The development of diagnostics has clearly benefited greatly from collaborations with many institutions.

Confinement Studies

- Magnetics for equilibrium reconstruction
- Diamagnetic flux measurement
- Thomson scattering (20 ch., 60Hz)
- CHERS: $T_i(R)$ and $v_\phi(R)$ (51 ch.)
- Neutral particle analyzer (2D scanning)
- FIReTIP interf'r/polarimeter (119µm, 4 ch.) [1]
- Density interferometer (1mm, 1 ch.) [2]
- Visible bremsstrahlung radiometer (1 ch.)
- Midplane tangential bolometer array
- X-ray crystal spectrometer: $T_i(0)$, $T_e(0)$

MHD/Fluctuations

- High-n and high-frequency Mirnov arrays
- Ultra-soft x-ray arrays (4) [3]
- 2-D x-ray detector (GEM) [3, 4]
- X-ray tangential pinhole camera
- Microwave reflectometers [2]
- Electron Bernstein wave radiometer
- Fast lost-ion probe (energy/pitch resolving)
- Fast neutron measurement
- Locked-mode detectors

Edge/divertor studies

- Reciprocating Langmuir probe [5]
- Fixed Langmuir probes (24)
- Edge Doppler spectroscopy (T_i, v_ϕ)
- Edge fluctuation imaging [6]
- 1-D CCD H_α cameras (divertor, midplane) [7]
- 2-D divertor fast visible camera [8]
- Divertor bolometer (4 ch.)
- IR cameras (30Hz) (2)
- Tile temperature thermocouple array
- Scrape-off layer reflectometer [7]
- Edge neutral pressure gauges [9]

Plasma Monitoring

- Fast visible camera [6]
- Visible survey spectrometer
- UV survey spectrometer
- VUV transmission grating spectrometer [3]
- Fission chamber neutron measurement
- Visible filterscopes [7]
- Wall coupon analysis [10]
- X-ray crystal spectrom. (astrophysics) [11,12]

Table 2.4 Major diagnostic systems on NSTX.

Collaborating institutions: [1] UC Davis; [2] UC Los Angeles; [3] Johns Hopkins University; [4] ENEA, Frascati, Italy; [5] UC San Diego; [6] Los Alamos National Laboratory; [7] Oak Ridge National Laboratory; [8] U. Hiroshima, Japan; [9] U. Washington; [10] Sandia National Laboratory; [11] Lawrence Livermore National Laboratory; [12] Massachusetts Institute of Technology.=======

Some recent highlights in diagnostic development are listed below.

- The multi-point Thomson scattering (MPTS) diagnostic for the electron temperature and density profiles was upgraded from 10 to 20 spatial points by rearranging the input optical fibers and adding polychromators and detectors. The additional channels provided greater resolution of the profiles of the electron density and temperature, particularly in the plasma edge. This was important for studies of the H-mode of operation, which were a focus of the experimental program in FY 02.

- The capability for scanning the line-of-sight in both the horizontal and vertical directions was added to the neutral particle analyzer (NPA). This instrument is capable of detecting neutral deuterium and hydrogen atoms escaping from the plasma with energies from 0.25 to 300 keV, which spans the range from thermal ions to above the neutral beam injection energy, with a time resolution of 1 ms. The spatial scanning allows the ion distribution to be probed as a function of energy, space and the pitch angle of the ion orbits, which is important for assessing the confinement of ions. This diagnostic provided unique measurements of the interaction of RF waves with the fast ions resulting from NBI.

- In collaboration with LANL, an ultra-fast visible camera was employed to measure the structure of turbulence in the plasma edge through the technique known as "gas-puff imaging". The new camera, built by Princeton Scientific Instruments, is capable of recording up to 28 images of 80 × 160 pixels at 10 μs/frame. The camera viewed the plasma edge near the outboard midplane along lines of sight roughly parallel to the local magnetic field in the vicinity of a manifold that injected brief bursts of helium or deuterium gas into the plasma edge. During gas puffing from the injector, two-dimensional images of the spatial distribution of the helium or hydrogen line emission in the plane perpendicular to the local field were obtained. Because of the high frame rate of the camera, it was possible to track the motion of persistent, moving structures, commonly called plasma "blobs", in the edge region.

- A collaborator from the University of Hiroshima, Japan, installed a second camera capable of recording at 47000 frames per second (~ 20 μs/frame) to view the divertor in visible light. This camera revealed long, fluctuating filamentary structures roughly following the direction of the magnetic field into the divertor.

- The fast reciprocating probe developed by collaborators at the University of California, San Diego, was commissioned and used to measure the profiles of the electron temperature and density and the plasma floating potential in the edge region. The fluctuations in the probe signals reveal intermittent events, which appear to be related to the "blob" structures seen in the images of the edge turbulence.

- A two-dimensional detector for soft x-rays based on a gas electron multiplier built by collaborators from the ENEA Laboratory, Frascati, Italy and Johns Hopkins University was installed in a pin-hole camera to view the plasma tangentially near the midplane. The images from this detector showed the

development of coherent structures in the x-ray emission from the core of the plasma characteristic of certain types of MHD instability.

- Vibration problems that had been encountered in the initial operation of the UC Davis far infrared tangential interferometer and polarimeter (FIReTIP) were eliminated, and the line integral density was routinely measured with high time resolution along the two sightlines that were instrumented. Excellent agreement was obtained with the absolute line-integral density from Thomson scattering density profiles. Preliminary measurements of Faraday rotation were also made. It is planned to incorporate these data into the EFIT analysis when some sources of noise and uncertainty on the polarimetry measurement are removed. Two additional channels were installed prior to the FY 03 run, bringing the FIReTIP to a total of four sightlines through the plasma.

- After modifying some of the lower divertor plates to provide access a dedicated x-ray crystal spectrometer was installed to perform studies of x-ray line radiation important to interpreting data from the Chandra and XMM/Newton astrophysical x-ray observatories.

- The integrated viewing and collection optics were installed for both the Motional Stark Effect (MSE) diagnostic (utilizing collisional fluorescence from neutral deuterium atoms in the heating beams) and the upgraded 51-channel CHERS diagnostic. The CHERS system which measures the ion temperature and toroidal flow profiles with high resolution was successfully commissioned in the early phase of the FY 03 operation. The ion temperature and toroidal rotation velocity profiles already reveal remarkable localized features under some conditions, likely associated with magnetic islands.

- A high resolution spectrometer was installed and commissioned to measure the poloidal and toroidal plasma flow in the edge from intrinsic C-III impurity and He-II emission. This diagnostic revealed the slow development of a hot ion component at the plasma edge during HHFW heating and its very rapid decay after the heating pulse.

- A scintillator-based detector was installed to measure the energy and pitch angle of fast ions lost from the plasma at the outboard mid-plane (the sFLIP probe).

- A new antenna for measuring EBW emission was installed in collaboration with the OFES Diagnostic Initiative Program. This system incorporates a movable limiter to steepen the edge density profile locally in order to increase the mode conversion efficiency from the EBW inside the plasma to a propagating wave which couples to the antenna.

- New magnetic sensors (24 each B_r and B_z coils) were installed on the primary passive stabilizer plates for analyzing the growth and structure of resistive wall modes and locked modes.

2.2 Five-Year Facility/Diagnostic Plan

The NSTX facility and diagnostic plan is driven by the overall NSTX five-year program plan as show in Fig. 2.8. In support of the physics goals established in this plan, a program of upgrades to the facility and the diagnostics has been developed.

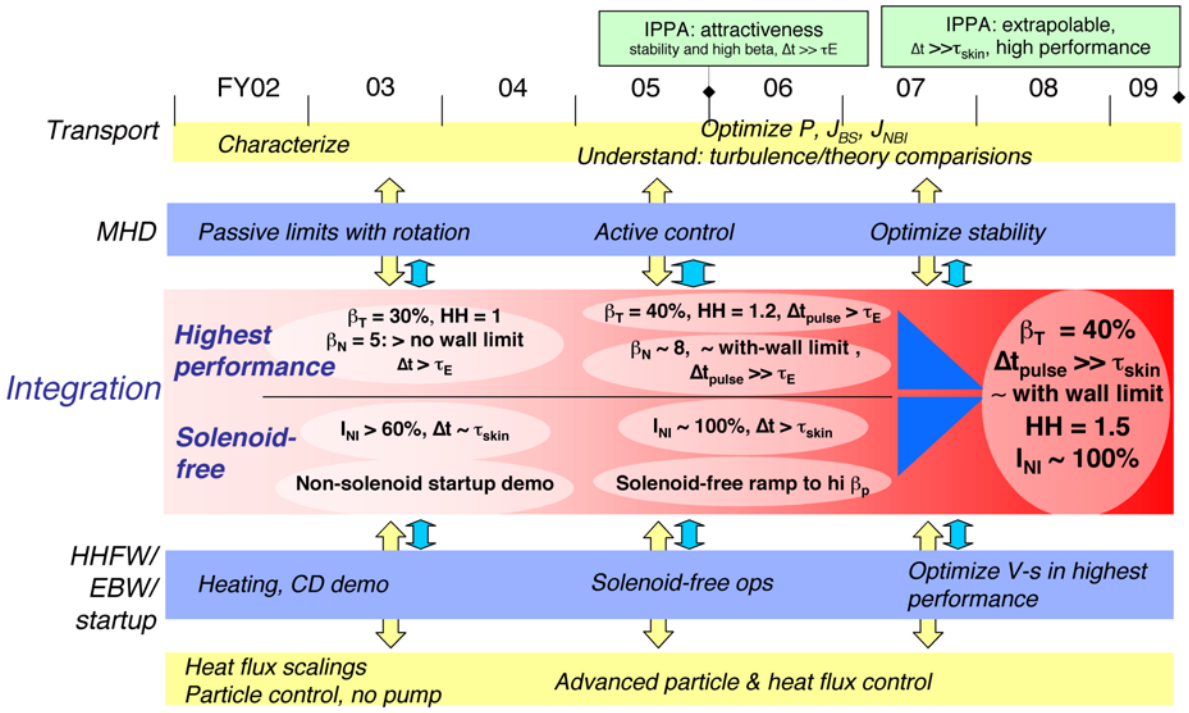

Fig. 2.8. NSTX Five-Year Plan Overview

2.2.1 Facility Upgrades

In Table 2.5 overleaf, the planned facility upgrades are listed. Each of the major upgrades is discussed in this and subsequent chapters. The lightly shaded areas represent the fiscal years in which design, fabrication and development, if required, occur, while the heavily shaded areas represent the fiscal years of installation.

Upgrade	Research Areas of Interest							Development/Installation					
	MHD	Transport	HHFW	EBW	CHI	Boundary	Integration	FY03	FY04	FY05	FY06	FY07	FY08
Auxiliary Systems													
Absorber field null control					√								
NB power modulation	√	√					√						
PF power supply upgrade	√		√				√						
HHFW antenna end-feed			√										
EBW system, 1MW	√	√		√									
EBW system, 3MW upgrade	√	√		√			√						
MHD/Error Field Control													
RWM sensors & detection	√						√						
Active mode-control	√						√						
PF1A coil modification	√					√	√						
Passive stabilizer relocation	√						√						
Fueling, Power and Particle Control													
Li/B pellet injector		√				√	√						
Supersonic gas injector		√				√	√						
Lithium wall coating	√	√	√	√	√	√	√						
Divertor cryo-pump		√	√	√	√	√	√						
D pellet injector (LFS)		√				√	√						
D pellet injector (HFS)		√				√	√						
CT injector		√				√	√						
Divertor long-pulse upgrade						√	√						
Liquid Li surface module	√	√	√	√		√	√						
Plasma Control													
D/A & processor upgrade	√		√	√	√		√						
Power supply response	√				√		√						
Real-time MSE, MPTS	√		√	√			√						
Real-time p(r), j(r) control	√	√	√	√	√		√						

Table 2.5. Proposed Facility Upgrades

Check marks indicate the topical areas which benefit from or are affected by the facility upgrades. The solid boxes indicate years when systems are installed; the shaded boxes represent years when development is underway or research supporting a design is performed.

2.2.1.1 Auxiliary Systems Upgrades

CHI Absorber Field Null Control

The near-term goal for the CHI system is to improve its reliability. In the past, internal absorber arcs and other external arcs have limited the progress in CHI. To solve the absorber arc problems, a new ceramic insulator assembly for the absorber was designed and installed during the FY 02 outage. A picture of the insulator ring and a schematic of the absorber section are shown in Fig. 2.9.

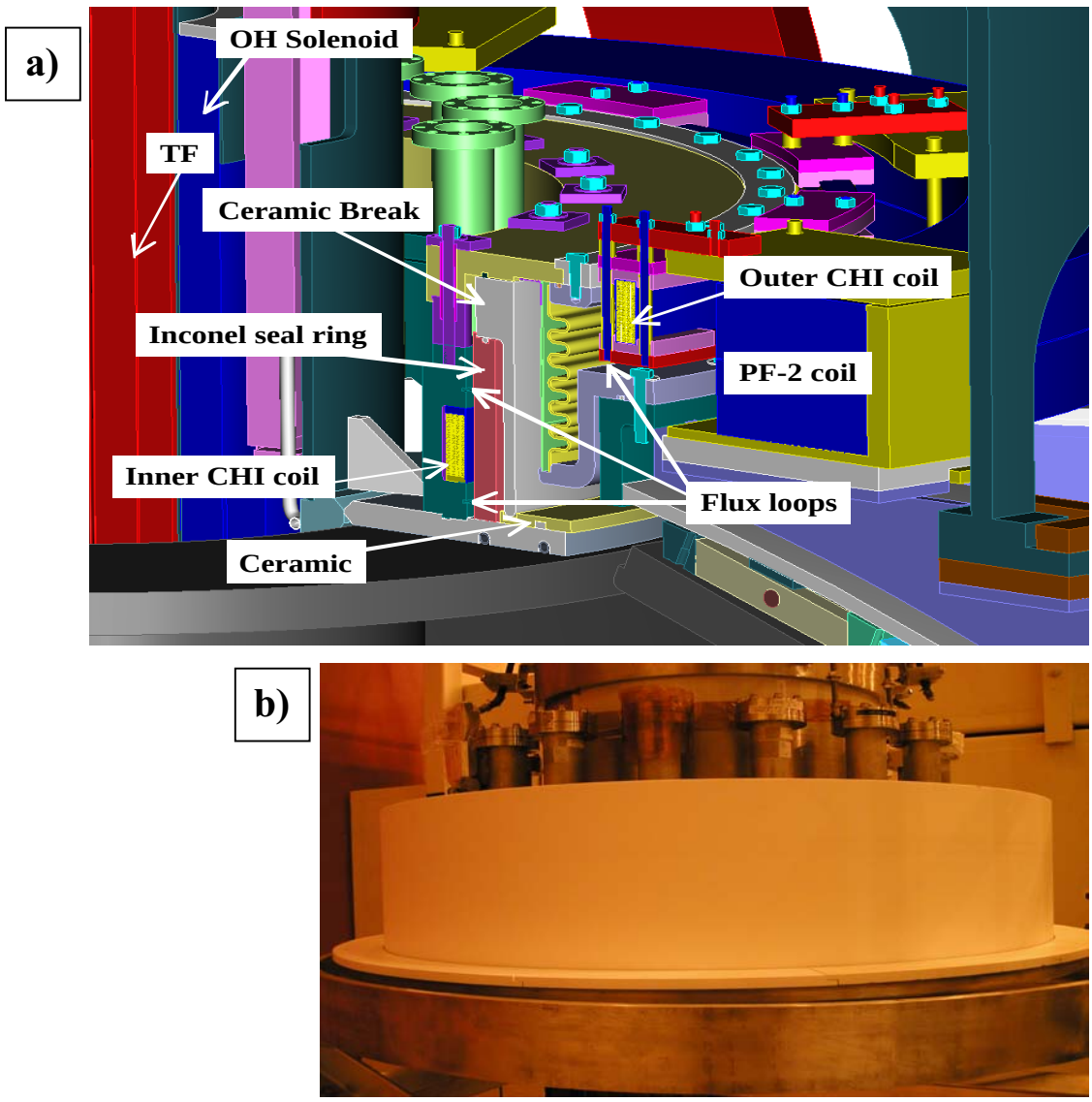

Fig. 2.9 (a) Cutaway view of the CHI absorber insulator and its surrounding structure including the new absorber field null control coils;
(b) The alumina insulator and the segmented annulus of boron nitride tiles covering the upper divertor flange ready for reinstallation of the center stack.

The new ceramic insulator incorporates the following improvements over the old design.

- Insulator on the high-field side – The original insulator on the low-field side probably suffered from plasma induced arcs because plasma entering the absorber tends to flow towards the low field region, so the new high-field-side ceramic insulator should suffer much less plasma contact. This configuration has been used successfully on the HIT devices.
- No simple connection path across insulator – Any arc must now follow a longer and more tortuous path.

In addition, two more small PF coils were installed in the absorber structure. These coils are designed to null the poloidal field across the absorber produced by both the other PF coils and the plasma itself during CHI. By nulling the local poloidal field in the absorber, the parallel connection length between surfaces at different potentials can be increased significantly. Flux-measurement loops were also installed to measure the local field near the absorber.

During the FY 02 CHI experiments, sporadic arcs had also occurred in components outside the vacuum vessel. In particular, breakdown occurred across the insulating sleeves which surround the bolts clamping the CHI ceramic insulator in the injector. These arcs appear to have started at the joint in the two-piece G-10 insulator. Those insulators have been replaced with a one-piece design. In addition, the voltage surge protection elements (metal-oxide varistors) were moved close to the injector gap to reduce the inductance of their connection because measurements showed that large high-frequency components (>1 MHz) developed across the injector gap during the CHI.

The CHI experiments conducted in the brief FY 03 run suggested that indeed the new absorber insulator is more resistant to arcs, but there was not sufficient run time to test it in conditions where arcs were unavoidable previously. Power supplies for the absorber field null coils will be installed and tested in FY 04 to add another level of arc suppression, if further experiments reveal that absorber arcs are still a problem. The power requirements for these coils are modest, although quite fast response is needed. A chopper power supply suitable for this application is being constructed by the University of Washington.

NBI Control System Upgrades and Power Modulation Capability

The NBI system, which consists of one beamline box and three ion sources from the TFTR system, has been the workhorse of the high-beta and high-confinement research in NSTX. Its reliability has been excellent and it has delivered up to 7 MW of heating power, well above the original 5 MW specified for NSTX. In FY 04, the NBI control system will be upgraded to enable finer adjustment of the average NBI power through duty-cycle modulation and to provide the capability for feed-back control of the heating power as part of the plasma control system.

PF Power Supply Upgrade

It is planned to commission additional power supplies for the NSTX PF coils to support the research, described in Sec. 3.4.b, into methods for plasma startup that do not rely on a central solenoid.. In particular, the PF4 coils in NSTX (which can be seen in Fig. 2.4 at R = 1.81m, Z = ±0.85m), which are presently not powered, can be combined with other PF coils to produce both a flux change in the plasma region and a poloidal field suitable for plasma startup and equilibrium without using the central solenoid. This would provide another means for initiating the plasma current in NSTX and raising it to several hundred kiloamperes where other means of non-inductive current drive could become effective. The commissioning of an additional power supply, cabling to the NSTX Test Cell and modification of the plasma and power supply control software to accommodate this coil will be undertaken in FY 04. If the initial tests of this scheme demonstrate promise, a bipolar capability would then be added to the power supply for the PF5 coils.

HHFW Antenna Upgrade

The NSTX HHFW system, designed in collaboration with ORNL, uses perhaps the most sophisticated high-power radio-frequency antenna employed to date in any plasma research device. In Fig. 2.10, we show a schematic of the RF power distribution network to the antenna elements. The phase of the RF current between the successive elements determines the wave-number spectrum of the launched waves. With the RF at 30 MHz, the parallel wave-number $k_{\parallel}$ of the launched waves can be varied from 14 m^{-1} to about 4 m^{-1}. The decouplers compensate for the large mutual coupling between neighboring antenna elements, permitting real-time feedback control of the spectrum to optimize the RF heating or current drive as plasma conditions evolve.

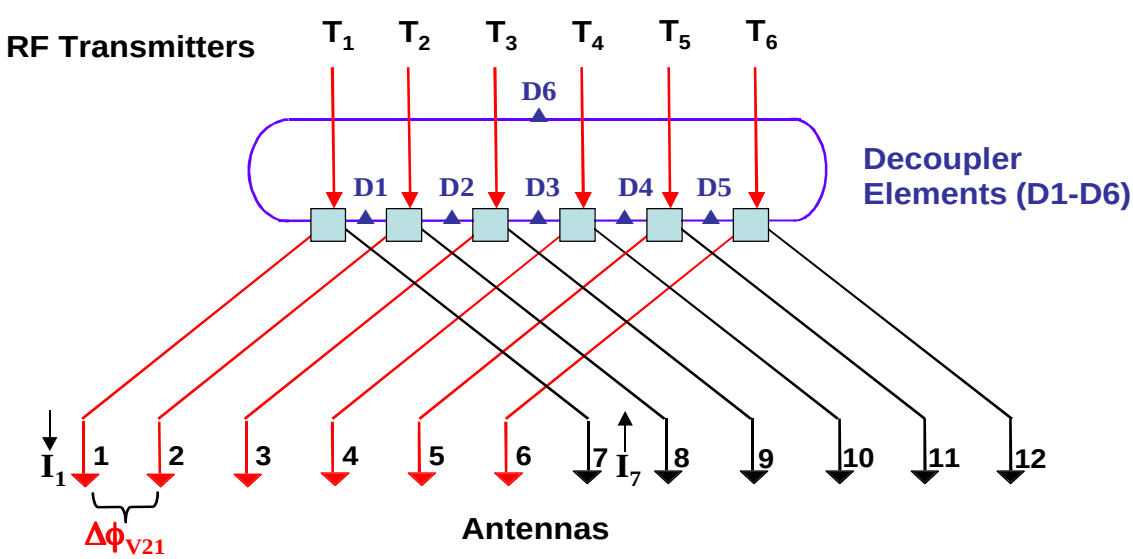

Fig. 2.10 Schematic of the digital phase feedback control system.

The phasing control implementation has been successful and the system has been operated with preprogrammed phase control in experiments to assess the HHFW-driven current. Progressing to feed-back control through the plasma control system should be relatively straightforward, once the plasma response to the HHFW power is well characterized.

At high RF power, the HHFW antenna has not been as reliable as desired. During operation with plasma, the antenna voltage stand-off significantly decreased from the levels achieved during vacuum conditioning. For the FY 02 experimental campaign, the power level was held below 3 MW due to arcing. Examination of the antennas during the FY 02 outage revealed arc tracks in the feed-through throat area. This feed-through design was based on the successful TFTR ICRF antenna. In NSTX, however, the radial diffusion in the scrape-off layer appears to be much larger, perhaps because of the low toroidal field, which allows plasma to penetrate the antenna enclosure and compromise the voltage stand-off. The problem may be worse during the RF pulse itself as evidenced by the pressure rise measured in the back of the antenna enclosure. To improve the situation, the antenna feed-through area was modified before the FY 03 run by thinning down the center conductor by about 5 mm in radius, thereby increasing the gap to the outer conductor by 50%, and adding a corona ring to smooth the transition region.

If further improvement is needed in the power handling, the antenna can be modified to use an end-fed, center-ground design. This would reduce the voltage on the feed-through by a factor of two at constant power or increase the power handling capability by a factor of four at constant voltage. In FY 04, the need for this will be assessed and, if necessary, a modification will be designed for installation in FY 05.

Electron Bernstein Wave (EBW) System

The EBW system for NSTX is envisioned as a tool to control the plasma current profile for long-pulse operation and for stabilizing neoclassical tearing modes (NTMs). NTM stabilization has been demonstrated in tokamaks with the localized current driven by electron cyclotron waves, but this method is not available in the “over-dense” ST plasmas. The EBW system for NSTX will also assist in non-inductive plasma start-up. The development of an EBW-CD model to optimize the design of this system, including the necessary mode-conversion between the electrostatic EBW and a propagating electromagnetic wave in the plasma edge, is being guided by measurements of the thermal EBW emission in both NSTX and CDX-U and by EBW experiments in the MST and Pegasus devices at U. Wisconsin.

The RF frequency for EBW current drive (EBW-CD) in NSTX will be approximately 15 GHz for absorption both at the fundamental and the Doppler shifted second harmonic of the electron cyclotron frequency. A launcher for this frequency is being designed that will allow control of the wavenumber spectrum and the polarization of the electromagnetic launch wave for optimum conversion to the EBW in the plasma. A steerable-mirror launcher combined with a rotatable reflective grating polarizer is being

considered, since this provides flexibility for optimizing the EBW coupling and controlling the EBW power deposition. An array of such launchers is being tested on MAST in 2003-4 and the results from this research will contribute to the NSTX design

Although there are presently no high-power sources available commercially in the frequency range of interest for EBW-CD, gyrotron technology, which has already been developed for higher frequencies, can be adapted in a relatively straightforward fashion for a 1 MW source at 15 GHz. This source development will begin in FY 04, along with the engineering design of the EBW-CD system, including the power transmission lines and the coupler. A TFTR neutral beam power supply is available to provide power for these tubes, but a modular solid-state regulator will need to be procured. The transmission system would use TE02 to HE11 waveguide converters at the tube outputs and low-loss corrugated HE11 waveguide from the gyrotron enclosure to the launchers. In FY 05, the system and related infrastructure will be constructed. In FY 06, the initial 1 MW system will be installed and experiments will begin. The upgrade to the full 3 MW system will continue through FY 07 with the full capability available in FY 08. The EBW research plan is discussed further in Chapter 3, Section 3.3.

2.2.1.2 MHD and Error-Field Control

RWM Sensors and Detection

A set of 48 sensors (12 each B_r and B_p coils mounted on the primary passive plates above and below the midplane) had been installed prior to the FY 03 experiments for characterizing the RWM and intrinsic error fields for the design of a suitable correction coil system. However, the premature termination of the FY 03 run precluded making measurements in conditions where the RWM has previously been observed.

RWM/Error Field Correction Coil System

The Resistive Wall Mode (RWM) and Error Field Correction Coil System is being described in detail in the MHD section (Chapter 3) and therefore will not be covered in detail here. As shown in Fig. 2.11, a set of six “picture frame” coils will mounted outside but close to the vacuum vessel near the outboard midplane, and will be connected as three opposing pairs to generate a radial field. These coils will be installed in FY 04. They will be used initially to cancel intrinsic “average” error fields generated by the various PF coils by applying time-varying currents in response to the measured PF coil currents. An assessment is currently being made whether to use additional rectifier power supplies of the type already used for the other PF coils, or to install faster switching power amplifiers (SPAs). After the effectiveness of the “average” error-field correction scheme has been evaluated experimentally, fast, active feedback based on real-time detection and analysis of the RWM will be implemented in FY 05–06 if needed.

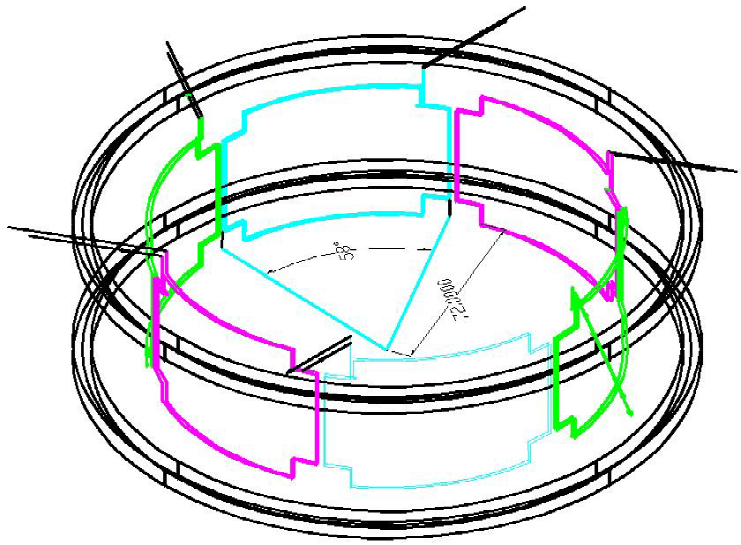

Fig. 2.11 Layout of proposed RWM control coils for NSTX. The axisymmetric coil bundles are the PF5 coils which control radial equilibrium

Modification of the PF1a Coils

Both the NSTX experimental results in FY 02 and recent modeling of discharge scenarios suggest that higher elongation and triangularity of the plasma cross-section are desirable for pursuing the advanced ST physics which characterizes the later years of this research plan. A study has been conducted of the benefits of dividing the present PF1a coils, which are elongated coils (radius 0.18 m, axial length 0.27 m, 48 turns each) mounted on the center stack in the "shoulders" at each end. By energizing only the outer half of each of these coils, it is possible to pull the X-point of double-null divertor plasmas inward and further from the midplane, increasing both the elongation and triangularity. An example of an equilibrium that can be produced using the outer half of the PF1a coil is shown in Fig. 2.12. As discussed in Chapter 4, such plasmas can have very high beta limits, with β_T exceeding 40%, and with good alignment of the bootstrap current for optimized pressure profiles.

Further physics studies are now underway to determine the split of the PF1a coil to optimize the performance of the resulting equilibria in terms of stability and the effectiveness of the bootstrap current. In FY 04, engineering analysis and design will be undertaken and the coils will be fabricated for installation in FY 05.

The change in the plasma configuration will affect some of the other upgrades presented in this plan, most obviously the possibilities for a divertor cryo-pump and the plans for diagnostics for the divertor region. These upgrades will be considered together in making a decision to proceed with the PF1a coil reconfiguration.

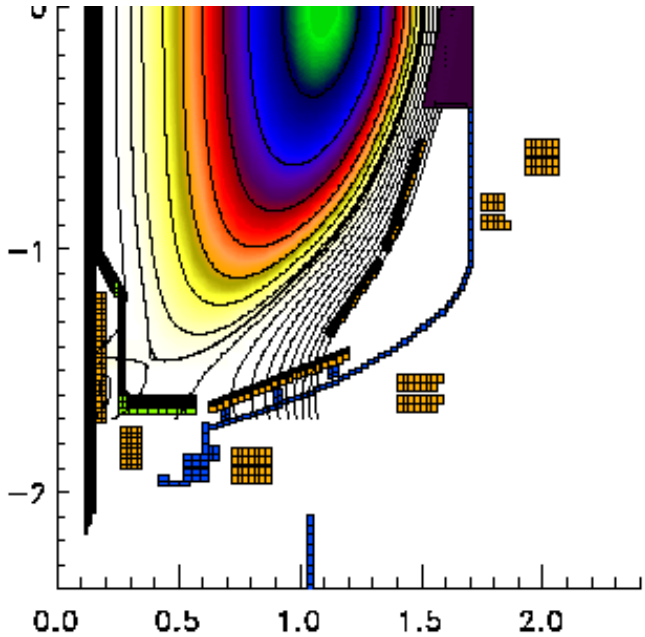

Fig. 2.12 Lower half of the cross-section of an equilibrium with high elongation and triangularity ($\kappa = 2.4, \delta = 0.8$) produced by using only the outer halves of the PF1a coils.

Secondary Passive Plate Modification

As the focus shifts toward higher triangularity, there may be a need to bring the secondary passive plates (*i.e.,* the plates further from the mid-plane) closer to the plasma boundary to maintain their effectiveness in suppressing instabilities. The original configuration of the passive plates was designed to accommodate a wide range of plasma shapes, including low triangularity discharges.

In Fig. 2.13, a schematic of a possible re-configuration of the plates is shown. The existing plates are depicted unshaded. With this modification, the secondary passive-stabilizer plates become better aligned with the high triangularity plasma boundary which is advantageous for plasma MHD stability. Because they have fewer diagnostic sensors than the primary plates, moving the secondary plates is relatively straightforward, although the sightlines for several diagnostics will be affected and alternate views must be provided for these. This configuration would also permit operation at moderate triangularity ($\delta \approx 0.5$) with an effective divertor cryo-pump on the outboard side, as shown in Fig. 2.13 and discussed in the following section 2.2.1.3.

The basic scheme for relocating the plates will be developed in FY 03, the engineering design and fabrication will take place in FY 04, and the installation will take place during the summer of 2004 to be

ready for the FY 05 experimental campaign. The new configuration of the plates will be designed to be compatible with the installation of a liquid lithium module, as discussed in Sec. 2.2.1.3.

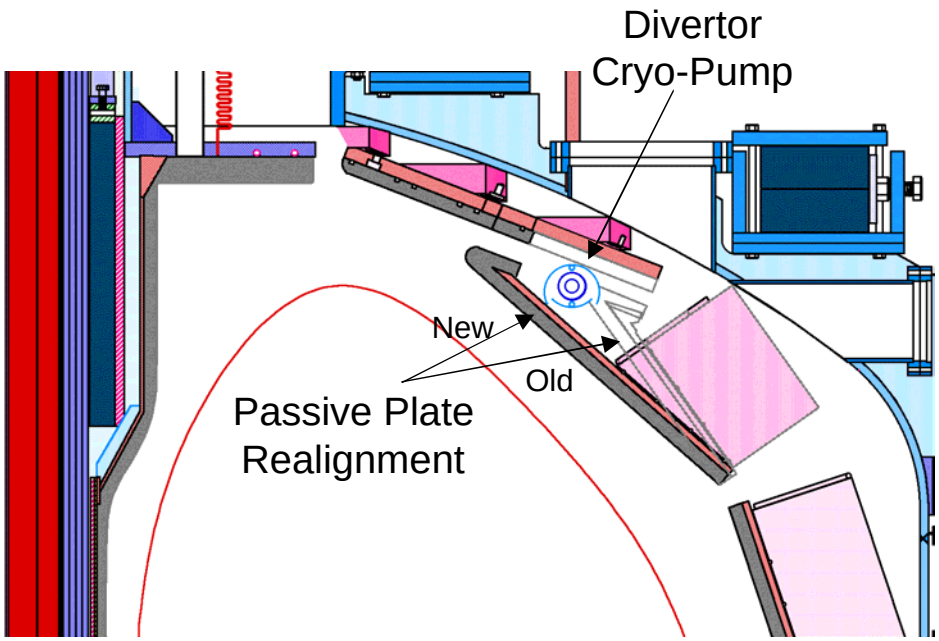

Fig. 2.13 Realigned Secondary Passive Stabilizer Plate. The possible outer location for the Divertor Cryo-pump (Sec. 2.2.1.3) is also shown.

2.2.1.3 Fueling, Power and Particle Control Upgrades

Control of gas recycling and impurity reduction have been the main emphases of boundary physics research thus far in NSTX. To these ends, the project implemented a variety of surface conditioning techniques including high-temperature bakeout, gas boronization, plasma boronization, and between-shot helium GDC. These contributed substantially to the achievement of excellent plasma parameters in NSTX. We anticipate incremental improvements to these techniques such as boronization during the bakeout and the rapid replenishment of boron films during a run day or even between discharges.

Gas puffing has been the primary method of plasma fueling in NSTX. The midplane high-field-side (HFS) gas injector installed in FY 02 improved the accessibility and quality of the H-mode. However, this injector suffered from the disadvantage that its flow rate was determined by the fill pressure before the shot and could not be modulated. An improved version of the HFS gas injector with better control capability was installed in the upper shoulder region of the center column for the FY 03 run. This injector revealed some differences from the midplane injector in the accessibility of the H-mode in different plasma configurations, but there was not sufficient time to investigate this before the FY 03 run ended. This investigation will continue into FY 04.

In this Five-Year Plan, the area of plasma boundary research shifts its emphasis to the issues of power and particle handling and advanced fueling to achieve the plasma performance needed for the planned advanced ST research. We now describe some of the key facility upgrades related to the plasma boundary to be undertaken during the five-year period.

<u>Lithium Pellet Injector</u>

The capability to inject small solid pellets and micro-pellet ensembles of lithium, boron, carbon, lithium deuteride, lithium carbide, or other low-Z elements at precise, controllable velocities will contribute to achieving a number of boundary physics goals, including wall conditioning, controlling disruption decay, and simulating some aspects of a liquid limiter. The pellets will also contribute to plasma diagnosis by enhancing charge-exchange signals, revealing edge impurity transport and enabling measurements of edge flows and rotation. A gas-driven Lithium Pellet Injector will be installed during the FY 03 outage with the capability for injecting solid pellets and micro-pellets (powder) at velocities from 20 m/s, for edge deposition, to 400 m/s, for deeper penetration.

<u>Supersonic Gas Injector</u>

Another tool being developed for NSTX is a supersonic gas injector. On Tore Supra, the edge recycling was significantly reduced by using a supersonic gas injector and its fueling efficiency was much greater

than that of conventional gas injectors. The benefits to NSTX are the possibility of achieving higher densities with lower recycling which could contribute to improved plasma operation in the near-term. Other applications include experiments on density profile control, triggering internal transport barriers, and control of MHD instabilities. Deeper penetration of neutrals may permit a wider edge barrier in the H-mode. There is also the possibility of using a supersonic injector for diagnostic purposes, such as impurity injection for transport studies, gas puff imaging of turbulence *inside* the plasma boundary, and edge temperature and density measurements based on spectroscopic line ratios.

In collaboration with the Mechanical and Aeronautical Engineering Department of Princeton University, a supersonic injector is being built and tested in the laboratory for installation initially on CDX-U in the summer 2003 of and then on NSTX. The graphite Laval nozzle of this injector is designed to accelerate deuterium gas, preheated to an inlet temperature of 373 K, to about 1.8 km/s, corresponding to about Mach 2 referenced to its sound speed at room temperature. The injector should be capable of delivering up to about 90 Torr.l of gas (6×10^{21} deuterons, *i.e.* about the total contents of a typical NSTX H-mode plasma) during a discharge. The nozzle will be installed on the outboard side on a movable mount to vary its distance to the boundary in order to study the effects of varying the gas density on the penetration through edge plasma. The supersonic gas injector will be available for the FY 04 NSTX experiments.

Lithium Wall Coating Capability

Several techniques are proposed for coating the plasma facing surfaces in NSTX with lithium. The aim is to achieve lower recycling and thereby to control the density rise which accompanies the good particle confinement in NSTX, particularly in the H-mode.

The first of these is to use the lithium pellet injector (discussed above) to introduce the maximum tolerable amount of lithium into the plasma edge by injecting multiple, low-velocity pellets, either prior to a high-power heating phase or in a series of preparatory discharges using the “painting” technique developed in TFTR. The lithium pellet injector will have the capacity to carry out a full day’s experiments with such operation on a single magazine of pellets. This capability will be available in FY 04.

Another technique being developed for deployment in NSTX is a lithium evaporator, which will be inserted into the vacuum chamber at appropriate intervals to deposit a fresh lithium film. An evaporator, which uses electron beam heating of lithium in a crucible and is small enough to be inserted on a movable probe, is being developed and tested on CDX-U for installation on NSTX in FY05, or possibly FY 04. If results from the initial evaporator are encouraging, an upgrade to provide uniform deposition in the divertor region will be undertaken.

Divertor Cryo-pump

High performance, H-mode plasmas are expected to continue as a standard operational scenario for NSTX. Since the density usually continues to rise in these plasmas through the accumulation of the NBI particles and recycling, density control techniques will be required to prevent the density from rising continuously during extended H-mode phases. The divertor cryo-pump is proposed to provide the particle handling required for non-inductively-sustained, long-pulse discharges,. Two schemes are being assessed.

First, a study has been performed by collaborators at ORNL of a cryo-pump mounted behind the secondary passive stabilizer plates, as shown in Fig. 2.13 in Sec. 2.2.1.2. This design is similar to that employed on DIII-D. Adequate pumping can be obtained for NSTX with this design if the throat of the pump is sufficiently close to the divertor strike point. With the secondary passive stabilizer plates in their present location, this would restrict efficient pumping to discharges with lower triangularity ($\delta < 0.3$) than is desirable for optimum stability. Thus, it would be advantageous to combine the installation of this outboard cryo-pump with the realignment of the secondary passive stabilizer plates proposed for FY 05. This scheme would then provide pumping for discharges with moderate triangularity ($\delta \sim 0.5$). Significant rearrangement of diagnostics would be required with this design since many sightlines and signal leads pass through this region.

The second scheme places the cryo-pump on the inner divertor plates, as shown in Fig. 2.14. This small-major-radius design is well suited for pumping double-null, high-triangularity plasmas, but their elongation may be restricted to prevent excessive heat fluxes to the cryo-pump shield. This implementation has the advantage that its installation would not be dependent on moving the secondary passive stabilizer plates nor involve displacing diagnostics on the outer vessel. The cryo-pump, its supply lines and the surrounding shield are all mounted on the center stack alone so that installation in NSTX will be relatively quick and minimally perturbing to other systems. In addition to providing pumping for high triangularity ($\delta > 0.7$) plasmas, it also provides the capability for pumping in the private flux region for lower triangularity plasmas to assess that scheme for controlling fueling through the X-point. This design must be optimized to handle the power flux to the shield during long-pulse operation.

Conceptual designs for upper and lower divertor cryo-pumps in both schemes are in progress prior to a decision at the end of FY 04 on the optimal scheme. The implications of subdividing the PF1a coils on the cryo-pump designs will be assessed as the analysis of the coil subdivision proceeds.

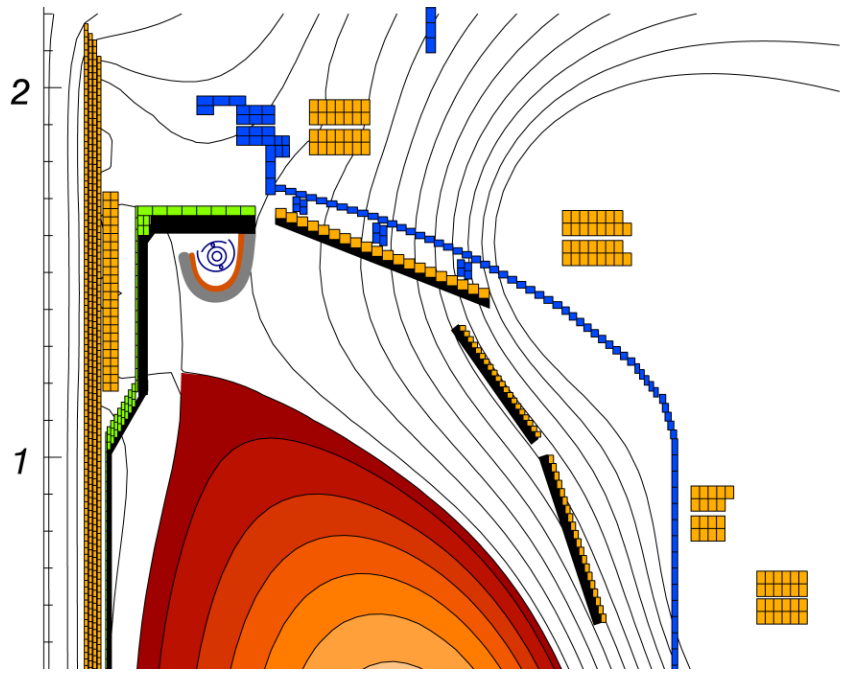

Fig. 2.14 Design concept for a divertor cryo-pump optimized for high-triangularity NSTX plasmas. The plasma cross-section is for a high-β H-mode discharge.

Deuterium Pellet Injector

In collaboration with ORNL, NSTX will install in FY 05 a multi-barrel, frozen deuterium pellet injector for studies of density profile control, and the initiation, development and diagnosis of transport barriers. The goal of the latter experiments is to produce density perturbations that trigger or lower the power threshold for transport barrier formation. Of particular interest and importance in ST plasmas is the reduction in electron heat transport observed in pellet-fueled plasmas in JET and elsewhere. In combination with edge pumping by a cryo-pump or a lithium-coated surface, pellet injection may provide a method to control the density profile and thereby to optimize the pressure and bootstrap current profiles.

The deuterium pellet injector will be installed at the end of the main pump duct (Bay-L). In addition to providing unguided injection at the plasma outer midplane, pellets from the injector mounted on the pump duct could be injected into the plasma near the inner wall using guide tubes. Injection of pellets on the high-field side of tokamaks has shown more centrally peaked fueling profiles due to the intrinsic drift of the ablation cloud surrounding the pellet outwards in major radius, *i.e.,* towards the magnetic axis. The capability for inboard injection will be installed in FY 06.

Compact Toroid (CT) Injection

In the longer term, fusion reactors may need a technique for fueling the plasma core directly. The CT injector is an attractive option for the ST configuration since it can take advantage of the relatively low magnetic field and strong field gradient for good penetration and localized deposition. CT injection was used successfully in experiments in the Tokamak de Varennes (TdeV) and this same single-shot injector is now available to NSTX. The injector must be reassembled, tested and qualified in the laboratory for eventual operation on NSTX. The CT injector is envisioned to become available for experiments on NSTX in FY 07. Ways in which this injector could be upgraded for multiple-shot operation in a single discharge will be explored while the injector is in the laboratory.

Long-pulse Upgrade to Divertor Tiles

The divertor surfaces of NSTX are currently ATJ graphite tiles. It is advisable to limit the surface temperature of these to 1200°C during the plasma pulse to avoid the phenomenon of radiation-enhanced sublimation from the surface, which can increase the influx of carbon into the plasma and eventually cause an uncontrolled carbon influx or "bloom". During the FY 02 run, measurements of the tile surface temperature with an infrared camera suggested that this operational limit may be exceeded if the present heat fluxes persist and the pulse length is extended beyond about 3 s for the advanced ST research planned for FY 07 and beyond. Various schemes for mitigating the heat flux, including strike-point sweeping and promoting divertor radiation, will be investigated in FY 04–05, as described in Ch. 3, Sec. 3.5.3b. If these do not achieve an adequate reduction in the heat fluxes, the divertor tiles will be upgraded to an advanced material, such as carbon-fiber composite, a refractory metal or possibly a metal coated with lithium. The tiles will be designed and fabricated in FY 06 for installation in FY 07.

Liquid Lithium Surface Module

A new possibility for particle removal, that also has potential for power handling, is the liquid lithium surface module (LSM). The effectiveness of the particle pumping for such a module is based on measured hydrogen retention rates in liquid lithium that approach 100%. It has been predicted that new, highly stable plasma regimes, with flat electron temperature profiles and high edge-temperatures, may be achievable with the extremely low edge recycling the LSM can provide. Indeed, simulations for NSTX with the UEDGE code by T. Ronglein of LLNL show that a reduction of the global recycling coefficient from 1 to 0.1 would reduce the density just inside the separatrix by a factor of 3 – 5, and increase both the electron and ion temperatures by a comparable factor without affecting the heat flux to the divertor significantly.

A major effort involving national laboratories and universities, called the Applications of Liquid-plasma Interactions Science and Technology (ALIST) Working Group supported by the Virtual Laboratory for Technology (VLT), is developing the LSM as an enabling technology for NSTX. The goal of the design is to exhaust $(2 – 5) \times 10^{21}$ deuterons/s for up to 5 s, by arranging a liquid lithium surface close to the plasma. One concept for a toroidal sector LSM of about 1 m^2 is shown in Fig. 2.15. Multiple modules would be installed to provide pumping of the full particle flux to the lower outer divertor. A full toroidal lithium tray is being tested as a limiter surface in CDX-U, and has already produced dramatic reductions in the hydrogen recycling and the virtual elimination of oxygen impurities.

The proposed LSM for NSTX will test capabilities that can then be scaled to the full requirements of fusion plasmas. Calculations, based on the measured temperature dependence of lithium evaporation rates, indicate that, for the power fluxes expected on NSTX, liquid lithium flow rates of 7 – 12 m/s will be needed to avoid excessive surface evaporation. There are several concerns that have to be resolved before the LSM is implemented in NSTX. These include the effects of MHD and thermoelectric currents in the liquid lithium, and the consequences of ELMs and disruptions. Extensive experimental and computational work is in progress to address these issues. The final decision for the implementation will be made in FY 06 based on the design/modeling and the experimental results from concept exploration experiments such as those being performed on CDX-U.

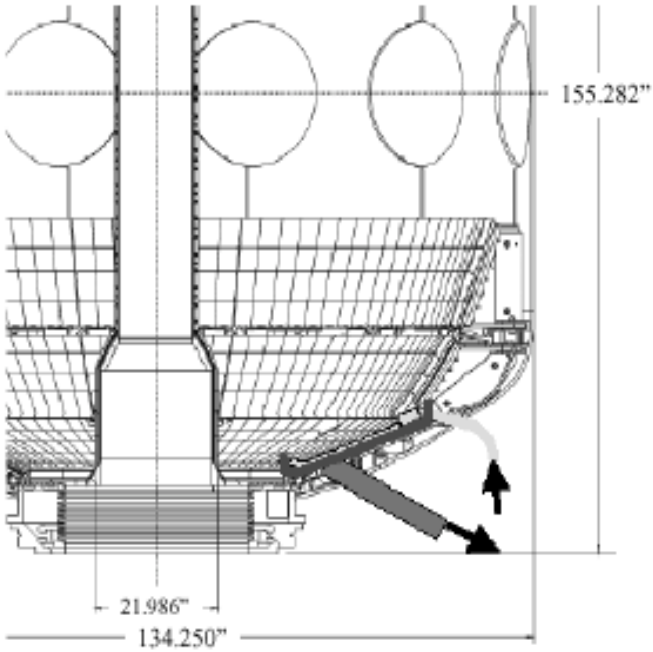

Fig. 2.15 Liquid Lithium Module Concept

2.2.1.4 Plasma Control Upgrades

Advanced plasma control is central to the research planned for NSTX over this five-year period. As the number of actuators for plasma control grows, there will be a corresponding growth in the requirements for real-time data acquisition and processing of these data to provide feedback on increasingly complex quantities, including profiles, related to the confinement, stability and operational regime of the plasma. The design of the real-time control system and plans for upgrades to it are described in Sec. 3.6 in the subsequent chapter so they will not be covered here in detail. They are listed in Table 2.5 to show their relationship to the other facility upgrades and to the research plans and emphases outlined in Fig. 2.8.

2.2.2. Computer and Data Acquisition Systems

The NSTX instrumentation and control (I&C) capabilities have been growing rapidly with the increased sophistication of the plasma diagnostic and control systems. The NSTX I&C system is composed of a process control and monitoring infrastructure, known as EPICS, the real-time plasma control system, a dual computer network, inter-system communications and data transfer for secure and open subsystems, a safety interlock and access control system, and a master timing and synchronization system. The MDSplus data acquisition system provides for sampling, acquisition, storage and display of diagnostic data, and synchronization of data sampling. The MDSplus system also provides for easy exchange of data between institutions and streamlines the application of standard codes to NSTX.

In Fig. 2.16, the rapid increase in the volume of data acquired from NSTX is illustrated. The pace of the expansion will continue as more advanced diagnostics are implemented and as the pulse length increases. A decision was made early on that all data should remain available on line throughout the life of the project. This has already proved very valuable in comparing new results with older data and in building databases to test hypotheses and assess trends. As a result, the online storage requirements are expected to increase each year by about 100 MB/shot for the foreseeable future. Fortunately, developments in data processing and storage technology are making it possible to keep up with this growth.

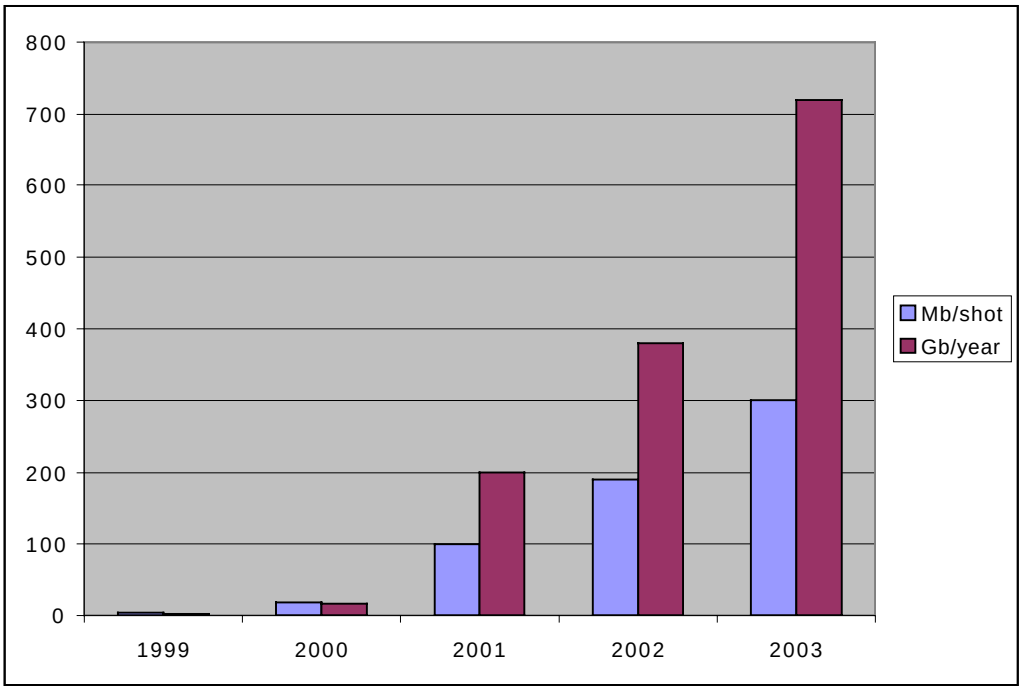

Fig. 2.16 Growth in the data acquisition volume on NSTX. The total per year for 2003 was projected for the planned 12-week run.

During its early operation, NSTX took advantage of large amounts of CAMAC equipment available from the preceding TFTR project. A total of six CAMAC highways, three for diagnostic data acquisition, two for facilities and one for the NBI system, provide communications to the primary control computers. The number of CAMAC crates on line grew rapidly to over 90, but this growth has now slowed as cheaper alternatives have become available. The project is now installing data acquisition systems based on basic PCs, ruggedized to function reliably in the NSTX environment, with commercial PCI and CPCI (a crate-based implementation of the PCI bus architecture) modules for almost all new diagnostics. The existing CAMAC installations will continue to be used until they are upgraded or the maintenance required for obsolete equipment becomes an issue.

One issue for eventually phasing out the CAMAC equipment has been a suitably accurate and flexible replacement for the facility clock system developed for TFTR using specialized CAMAC modules. The Engineering Division has recently developed and tested in the laboratory a PCI-based implementation of the clock modules, based on field-programmable gate arrays, which reproduce all of the functions of the CAMAC clock modules. A user interface based on LabView has been developed and one for Linux based PCs will shortly be developed. The first field deployment and testing of these modules will be made in FY 03 and they will then become standard for all new installations.

The MDSplus data has until now been managed and served by computers running the VMS operating system. However, the cost of mass storage using Raid-5 arrays is now higher for VMS-based than for LINUX-based systems, where costs have fallen to under $10K/TB. The first LINUX-based server for NSTX data will be brought on line later this year and a migration to these servers for all new data will take place in the next few years.

NSTX is participating in the development of large-scale multi-processor computing facilities at PPPL, having purchased nine dual-processor LINUX-based units for the (currently) 140 unit PETREL cluster. The analysis software for the data from the NSTX multi-point Thomson scattering diagnostic has been parallelized and is now run on that cluster. As a result, fully analyzed profiles of the electron density and temperature as a function of time are now available about 2 – 3 minutes after an NSTX shot (compared with 7 – 8 minutes on a single processor). The limitation on processing time is now largely in reading the raw data from the local digitizer memory. The migration of analysis tasks to the multi-processor cluster is expected to accelerate in the next year.

A 100Mbps network infrastructure, which is now at full capacity, is the primary path for data analysis on the UNIX cluster and for data distribution and access. This path will be upgraded to Gigabit Ethernet for the FY'04 experimental run. Further Gigabit upgrades will be required in the NSTX network infrastructure to support additional MDSplus servers and increased bandwidth between the Control Room

and D-Site where the experiment is located. An NSTX diagnostic fiber infrastructure of 100 channels was completed in FY 01.

The Plasma Control System using the multi-processor SkyBolt II™ computer was expanded in FY 02 using FPDP Input Multiplexing Modules (FIMM) developed at PPPL to provide direct memory access to the SkyBolt II for many additional data channels over one fiber link. A detailed description of the plasma control system is given in Section 3.6.

2.2.3. Diagnostic Upgrades

As described in Sec 2.1.4, the priority during the initial phase of NSTX operation has been implementing diagnostics to measure the basic plasma properties. The diagnostic upgrades planned for this five-year period include a steady improvement of these basic measurements, often utilizing established techniques. An example is the planned upgrade to the prototype divertor foil bolometer to multiple views to enable tomographic reconstruction of the divertor radiation. However, because of measurement challenges peculiar to the ST, or advanced physics needs, the upgrade plans also include innovative advanced diagnostics that are more developmental. Present plans for a motional Stark effect polarimeter operating at the low fields in NSTX and for a high-k microwave-scattering diagnostic capable of probing the turbulence believed responsible for electron transport fall into these categories.

Using experience-based estimates, this plan for diagnostic upgrades has been constrained to provide a reasonable profile of upgrade costs. Accommodating all the proposed diagnostic upgrades is a significant challenge. Port space is already crowded at the midplane, although the situation is significantly better for the upper and lower ports, where some ports are currently unused. Plans for relocating existing diagnostics or integrating uses of port space have been made for some of the proposed upgrades and there are plans to add some small ports at or near the midplane. Adequate staffing will also be needed to maintain and operate the planned diagnostics. However, diagnostic staffing levels are not projected to increase in proportion to the number of upgrades, as a result of improvements in productivity and automation.

The diagnostic upgrade plans are summarized in Table 2.6 overleaf. Once again, the lightly shaded areas represent the fiscal years in which design, fabrication and development, if required, occur, while the heavily shaded areas represent the fiscal years of installation and deployment. Depending on the nature of the upgrade and whether its installation and calibration require a major opening of the vacuum vessel, the diagnostic may become available for experiments in the year of deployment or the following year. Note that the upgrades for FY 03 to FY 07 are presented since these will benefit the research plan for FY 04 through FY 08. Descriptions of the planned upgrades are then provided in the following paragraphs, broadly categorized by the research areas that most benefit from these new tools. Many of these diagnostic upgrades will be carried out by or jointly with collaborators from other institutions. These are indicated in the text where specific collaborations have been proposed. In many cases, the implementation of these upgrades is dependent on the success of these collaborators in obtaining funding both for the specific diagnostics and for their associated research programs. Other collaborations may develop during the course of this plan as expertise and interest grows at other institutions.

Upgrade	Research Areas of Interest							Development/Deployment				
	MHD	Transport	HHFW	EBW	CHI	Boundary	Integr'n	FY03	FY04	FY05	FY06	FY07
Additional magnetics	√		√		√	√	√					
Imaging x-ray crystal		√										
EBW antenna with local limiter												
Fast lost-ion probe	√	√										
CHERS (51ch)		√				√	√					
MSE/CIF (10ch / 19ch)	√	√	√	√	√		√					
Additional x-ray cameras	√				√		√					
FIReTIP upgrades	√	√	√	√	√	√	√					
Line-filtered cameras		√				√						
Microwave tangential scattering		√										
Microwave backscattering		√										
MPTS (30ch / 90Hz / 40ch)	√	√	√	√	√	√	√					
Fast reciprocating probe	√	√	√	√		√						
Horiz. divertor bolometer						√	√					
Edge Doppler upgrade	√	√	√	√	√	√	√					
Deposition monitors						√						
Poloidal CHERS	√	√					√					
MSE/LIF	√	√	√	√	√		√					
Planar LIF visualization	√	√				√						
Neutron collimator		√										
Langmuir probe upgrades						√						
Divertor visible spectrometer						√						
Fast IR camera					√	√						
Vert. divertor bolometer						√	√					
Imaging reflectometer	√	√										
Helium-jet spectroscopy						√	√					
Divertor reciprocating probe						√						
Charged fusion product det'r	√	√										
Divertor Thomson scattering						√	√					
Divertor UV spectrometer						√						
Energy extract analyzer						√						

Table 2.6. Diagnostic upgrades planned to support NSTX research in FY 04 – FY 08.

2.2.3.1 MHD Diagnostics

Enhanced magnetics – The externally mounted locked-mode coils installed in FY 01 were instrumental in detecting performance-limiting MHD instabilities caused by intrinsic error fields on NSTX. During the 2002 summer outage, a more extensive set of 24 B_r coils was mounted around groups of tiles in the primary passive stabilizer plates, much closer to the plasma, to permit a more thorough investigation of error fields. These studies have been delayed to the FY 04 run by the TF coil failure. In addition, 24 large-area B_p coils were mounted on the edges of the primary passive stabilizer plates closest to the midplane. These will initially be used to detect and characterize resistive wall modes (RWM), and eventually to provide input to the planned RWM stabilization system (Sec. 2.2.1.2). These sensors will be ready for initial investigations in FY 04.

As seen in Table 2.6, it is anticipated that there will be continuing upgrades to the magnetic diagnostic set as the requirements for analysis and control evolve with the research program. Planned upgrades to the conventional magnetic diagnostics include a more comprehensive set of high-frequency Mirnov coils and fast digitizers to resolve fluctuations in the range of harmonics of the ion cyclotron frequency.

A 1-D set of sensors to measure the distribution of current flowing from the plasma to the wall tiles, I_{wall} *vs.* Z along the center stack, will be installed to aid in magnetic reconstruction of the plasma equilibrium during CHI.

Additional SXR cameras – Researchers from Johns Hopkins University have installed a number of 1-D soft x-ray cameras at two toroidal locations on NSTX. Two types of cameras are used, larger systems with discrete absolutely calibrated extreme-ultra-violet (AXUV) diode detectors, and compact systems employing AXUV diode arrays. These detectors are sensitive in the range 10 eV – 10 keV. Foil filters are used to select the energy range of interest for specific experiments. Over the next two years, additional compact arrays will be implemented to improve the capability for tomographic reconstruction of the ultra-soft x-ray emission profile to resolve smaller-scale MHD perturbations. Johns Hopkins University has also proposed a novel concept for a continuous high-speed x-ray pinhole camera utilizing ASIC chip technology for data acquisition. In this concept, light is transported, by high efficiency light guides, from a high efficiency CsI(Tl) scintillator to a series of multi-anode (8 × 8) photomultipliers or avalanche-photodiode arrays. Outputs are connected to 128 channel ASIC data acquisition boards performing simultaneous charge integration, digitization, and readout. These boards are currently capable of 10 kHz readout but will be upgraded to 100 kHz continuous operation later.

Recently, a tangential pinhole camera utilizing a 12 × 12 pixel Micro Pattern Gas Detector (MPGD) with a Gas Electron Multiplier (GEM) as an amplifying stage was installed, in collaboration with ENEA Frascati (Italy) and Johns Hopkins University. Since each pixel is a proportional counter, the GEM gain

and discriminator thresholds can be used to select the x-ray energy range. Fast, low-noise electronics permit count rates to 10^7 photons/s/pixel and framing rates to 100 kHz. The 2.5 cm × 2.5 cm detector is easily moved behind the pinhole to change the location and size of the probed region. Recent results on NSTX were restricted, because of the 12 μm Be vacuum window, to energies 2.5 keV ≤ $E_{h\nu}$ ≤ 10 keV and frame rates ≤ 50 kHz for reasonable signal-to-noise (S/N) ratio. However, it is straightforward to utilize thinner windows, and thereby greatly increase the signals to achieve higher frame rates. A three-axis translation stage was recently installed for the detector to provide remote capability for pan and zoom. It also appears straightforward to extend this technology to higher pixel count cameras, and 32 × 32 pixel cameras are currently under development for installation in FY 04.

Princeton Scientific Instruments, Inc., in collaboration with PPPL, is developing a fast, high-resolution 2-D tangentially-viewing x-ray camera utilizing an ultra-fast CCD camera as a readout device. Similar to systems developed for TEXTOR and LHD, this system, shown in Fig. 2.17, features a wide-angle tangential view, variable pinholes and foils, a phosphor-coated faceplate vacuum interface, and a gated image intensifier tube with a fast phosphor. The electrostatic image tube demagnifies the 80 mm diameter phosphor image to match the 13 × 13 mm CCD size at the P46 phosphor anode. The output image is lens-coupled to the CCD. The camera is a PSI-Vmodel CCD with 64 × 64 pixels and 300-frame onboard storage capability with frame rates up to 500 kHz. The detector, which is currently being calibrated on the bench with an x-ray source, is scheduled for installation on NSTX in late FY 03. The data from this camera will be used to provide additional constraints on the EFIT analysis of the plasma equilibrium.

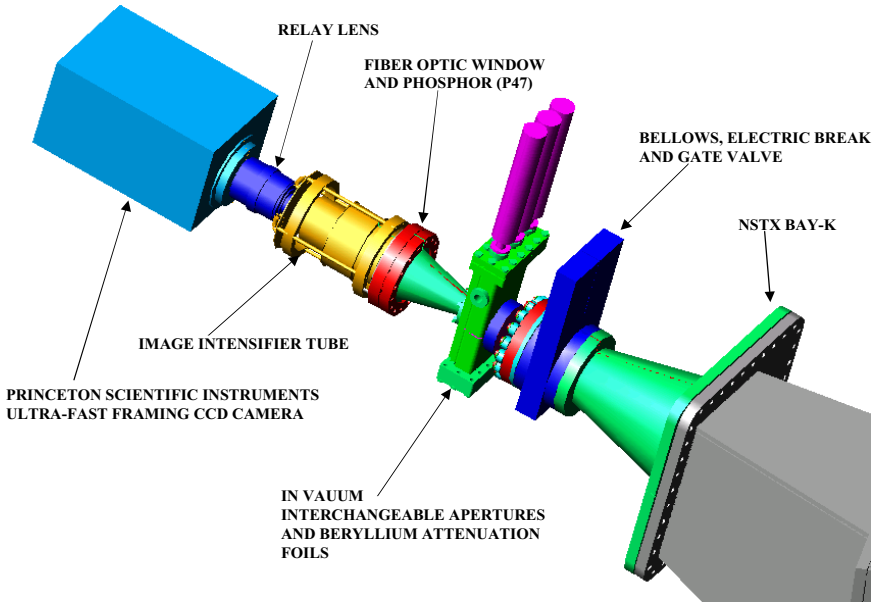

Fig. 2.17 Schematic of 2-D burst-mode tangential x-ray camera for NSTX.

Motional Stark effect polarimetry (MSE/CIF) – One of the major NSTX performance goals is the attainment of high β, long pulse discharges with a high fraction of non-inductive current. Measurement of the toroidal current density profile is critical to understanding both stability at high β and the role of non-inductive current drive. Considerable effort has been made, in collaboration with NOVA Photonics, to adapt motional Stark effect (MSE) polarimetry to provide this capability on NSTX. The first of two planned MSE diagnostics is currently being installed on NSTX. This system will use the collisionally induced fluorescence (CIF) arising from collisions between energetic D^0 atoms injected by the heating beam and the background plasma. Modifications have been made to improve resolution of the Stark polarization components, whose spectral splitting is reduced at the low B fields of the ST. First, the viewing aperture has been narrowed toroidally, thereby reducing the Doppler spreading of individual components due to the spread in viewing angles. Second, a high-throughput, narrowband birefringent Lyot filter has been developed with a bandpass of 0.061 nm FWHM, compared to the typical 0.7 nm bandwidth of a standard interference filter. Fig. 2.18 shows a photo of the four-stage filter. Even with these improvements, the polarization fraction of the detected light is predicted to be in the range 0.2 – 0.4, much smaller than the value of 0.8 typical for this technique on high-field devices. To compensate for the resulting loss in S/N, the optical throughput is increased for the NSTX system. Each of the 19 spatial channels receives light from 76 fibers 1 mm in diameter, which are imaged with aspheric optics through the Lyot filters and onto a 1.0 cm diameter avalanche photodiode. Spatial resolution will be 2 – 3 cm,

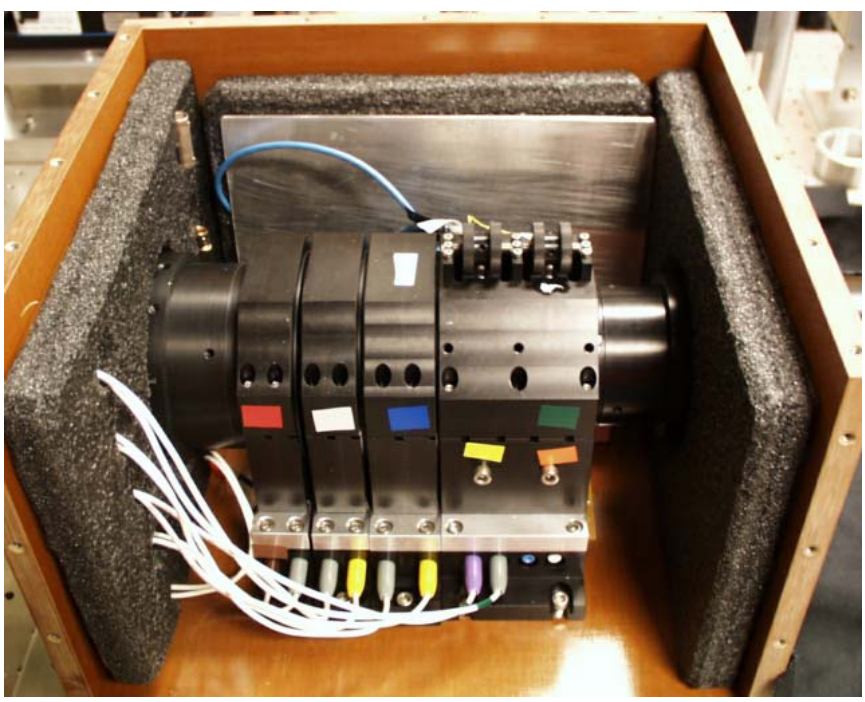

Fig. 2.18 Tunable Lyot filter and detector housing for MSE/CIF system

with coverage from 10 – 20 cm inboard of the magnetic axis to the outer edge. The collection optics, photoelastic modulators, and fiber optics were recently installed on NSTX, and filter/detector systems are being assembled and tested. The goal is to instrument 10 spatial channels by the middle of the FY 04 run with 9 additional channels following a year later.

Motional Stark effect polarimetry (MSE/LIF) – On a longer development path, a second MSE system is planned for NSTX with installation scheduled for FY 05, again in collaboration with Nova Photonics. This system will inject a dedicated compact H^0 beam coaxially with the beam of a tunable laser that can be made resonant with the Doppler shifted H_α transition for the beam atoms. The linear polarization of the laser beam is rotated and the phase between this rotation and the intensity of the laser-induced-fluorescence (LIF) is used to determine the pitch angle. This system is currently being developed in the laboratory. For NSTX the MSE/LIF system will use a 40 keV H^0 beam, being developed at Lawrence Berkeley National Laboratory, with an equivalent ion current of 30 mA and a diameter of 1.2 cm. To be feasible with practical laser powers, the H^0 beam needs to very mono-energetic, with a parallel energy spread of ~1 eV. The development effort for the beam is currently aimed at reducing ripple and RF noise in its power supply and at improving the RF ion source to minimize its thermal energy spread and to improve the atomic fraction of the beam. The laser is an argon ion pumped ring dye laser with a CW output of 0.8 W. A high throughput optical system will image the LIF onto 19 channels covering the outer half of the plasma with 2 – 3 cm resolution. The neutral beam for the MSE/LIF system will be injected radially to eliminate the effect of the radial electric field, E_r, on the determination of the pitch angle. In principle, since the conventional MSE/CIF measures the combined effects of E_r and B_θ, the data from both MSE systems on NSTX will permit determination of $E_r(R)$ as well as j(R). In addition to the E_r and pitch angle, the pressure profile can also be determined. This is based on measuring the absolute motional Stark shift and thus the deviation of the local field from the vacuum value caused by the plasma diamagnetism. With the MSE/LIF system, this can be done by scanning the laser in wavelength or alternatively, with a fixed laser wavelength, by varying the beam voltage to vary the Doppler shift.

EBW radiometry – Since in an ST, $\Omega_{ce} << \omega_{pe}$, the first several electron-cyclotron harmonics cannot propagate as electromagnetic waves and conventional radiometry of the thermal electron cyclotron emission is not possible. However, fast $T_e(R,t)$ measurements potentially valuable for MHD studies may be possible based on the electrostatic EBW, which are mode-converted to propagating electromagnetic waves at the upper hybrid layer in the scrape-off layer. Studies are underway on both NSTX and CDX-U to measure the mode conversion efficiency and its dependence on the density scale length at the upper hybrid resonant layer, L_n^{UHR}. On NSTX, mode conversion efficiencies as high as 40% have been observed, in agreement with model calculations based on the measured L_n^{UHR}. On CDX-U, a local, radially-scannable limiter has been used to modify L_n^{UHR} in the vicinity of the receiving horn, and thereby increase the conversion efficiency to near 100%, based on comparisons with core Thomson temperatures.

On NSTX, a similar receiving horn/limiter assembly was recently installed, shown in Fig. 2.19. Two radially moveable graphite limiters, oriented normal to the local field on either side of the receiver, will locally modify L_n^{UHR}. A second microwave horn will be used in a reflectometer to measure the local density profile evolution. First results from the new receiver will come in FY 04. These studies are important, not only for demonstrating the feasibility of EBW radiometry for fast $T_e(R,t)$ measurements, but also for gaining confidence in high-power EBW for heating and current drive of ST plasmas.

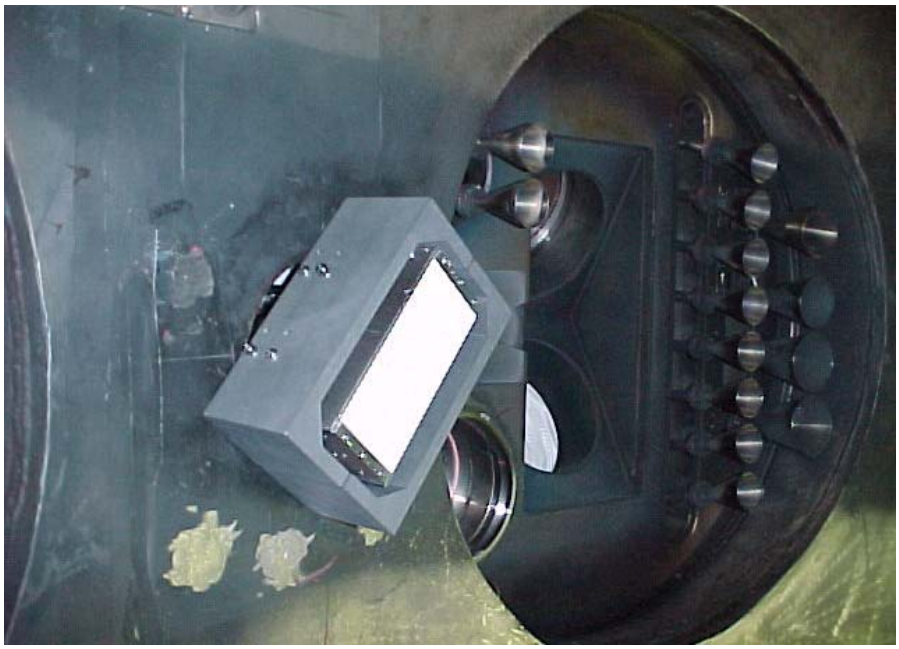

Fig. 2.19 Dual-horn EBW receiver/edge reflectometer (behind the white boron nitride shield) with movable graphite limiters in NSTX

2.2.3.2 Transport Diagnostics

Thomson scattering – The NSTX Thomson scattering system is modular and designed with collection optics expandable to provide up to 40 spatial channels and with input optical infrastructure to accommodate 3 Nd:YAG lasers. From the current 20 channel, 60 Hz (2 laser) configuration, upgrades are planned to go to a 40 channel, 90 Hz system over the next several years. There is particular interest in improving the coverage and resolution at the plasma edge, where a resolution of ~ 5 mm is possible.

2D Imaging x-ray crystal spectrometer – The present high-resolution x-ray spectrometer on NSTX measures the Doppler broadening and intensity ratios of lines emitted by highly charged states of argon along a single horizontal chord through the plasma center. This yields the central temperatures of both

ions and electrons with a time resolution of typically 10 ms through most of a discharge, and provides the advantage over the CHERS diagnostic of not requiring the injection of NBI (although doping with non-perturbing amounts of argon is needed). This is clearly a benefit for the study of plasma heated either ohmically or by HHFW auxiliary power. The x-ray spectrometer will be upgraded during FY 03 by adding a spherical crystal and a 2-D multi-wire proportional counter detector to provide spatial resolution over the range Z = ±40 cm from the axis.

Poloidal CHERS – Design work is underway for a charge-exchange recombination spectroscopy (CHERS) diagnostic to measure poloidal rotation on NSTX. In order to view vertically through the region of the plasma traversed by the heating beam, access slots will be cut through the outer divertor plates and secondary passive stabilizer plates, as shown in a 3-D model in Fig. 2.20. This system will be based on the same high-throughput, f/1.8 transmission grating spectrometers (Kaiser Holospec model) used in the NSTX toroidal CHERS system and in the edge Doppler system. High throughput and excellent S/N will be provided to achieve good spatial resolution through inversion of data from multiple sightlines that pass through the 40 cm tall heating beam. Initial data from this system should be available in FY 05.

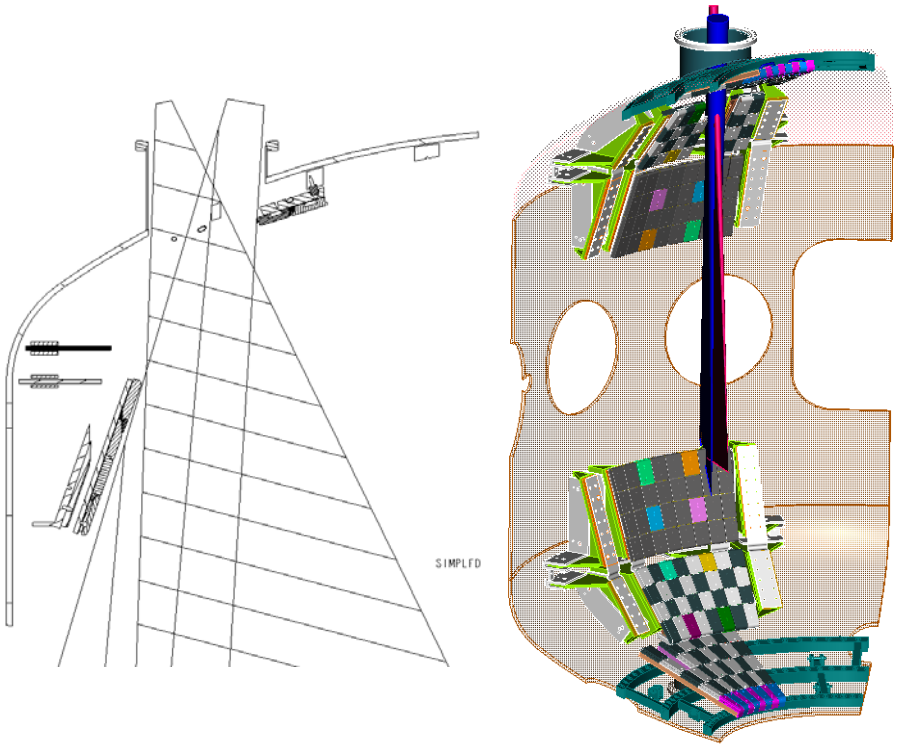

Fig. 2.20 Viewing concept for poloidal CHERS

FIR laser tangential interferometer/polarimeter – In collaboration with UC Davis, NSTX is developing a FIR laser tangential interferometer/polarimeter (FIReTIP), for fast measurements of electron density and the local toroidal field. The latter data will be used as additional constraints on the equilibrium analysis. This system currently has three channels instrumented in a midplane tangential fan and an additional four channels are planned. The changes to the launching port and the retroreflectors to provide these sightlines will be made when the vessel is modified for the microwave scattering system described in Sec. 2.2.3.3.

Neutron collimator – To measure the radial distribution of beam ions, it is planned to install a multi-channel neutron collimator in collaboration with UC Irvine. This system would employ seven horizontal sightlines in a tangential fan. A fairly massive collimating structure will be needed, and midplane space is available for this at the RF antenna bays. Laboratory development is underway to select the detectors and evaluate collimation schemes. A 3-channel prototype may be installed during the FY 04 run to provide design verification for the 7-channel system that is targeted for FY 05.

Solid-state fusion product detector – Another technique to measure the profile of the D-D fusion reactions is to detect the resulting 3 MeV protons whose orbits extend outside the plasma boundary. A multi-contact diamond detector or another type of multi-element solid state detector would be placed in the vacuum behind an aperture. The 3 MeV protons originating at a particular minor radius will produce a characteristic distribution on the detector elements at different locations. The source profile can then be unfolded using a numerical fit to a plasma equilibrium. This diagnostic will also be developed in collaboration with UC Irvine and researchers at TRINITI, Troitsk, Russia.

Fast lost-ion probe – On NSTX, the loss of fast ions injected by the neutral beams can be significant at low plasma current, particularly for plasmas with elevated central q, and is predicted to increase with β. To investigate this loss, a scintillator-based fast lost ion probe (FLIP) has been installed on NSTX, similar to those developed for TFTR. This probe, shown in Fig. 2.21, features an aperture located ~ 2 cm into the shadow of the RF limiter. Fast ions on loss orbits passing through the aperture hit a scintillator at a position on its surface that depends on their gyroradius and pitch angle. The emitted light is imaged through a vacuum window onto a coherent fiber bundle and relayed to an intensified CCD camera. A novel feature of this probe is that the detector plane is also divided into an array of 10 Faraday collector regions that are shaped to correspond to intervals of pitch angle. These Faraday collectors, which consist of aluminum layers deposited between the scintillator and its substrate, will provide higher time resolution and a simple means of absolute calibration for the 2-D optical detection system. Because the detector assembly is close to the plasma boundary and potentially subject to large heat fluxes, a heavy copper support is used as a heat sink to keep the P46 phosphor temperature below 200°C. Because of the low field and large gyro-orbits, the NSTX probe is ~ 8 times the linear dimension of the TFTR probes. Data from this probe will be available in the FY04 run.

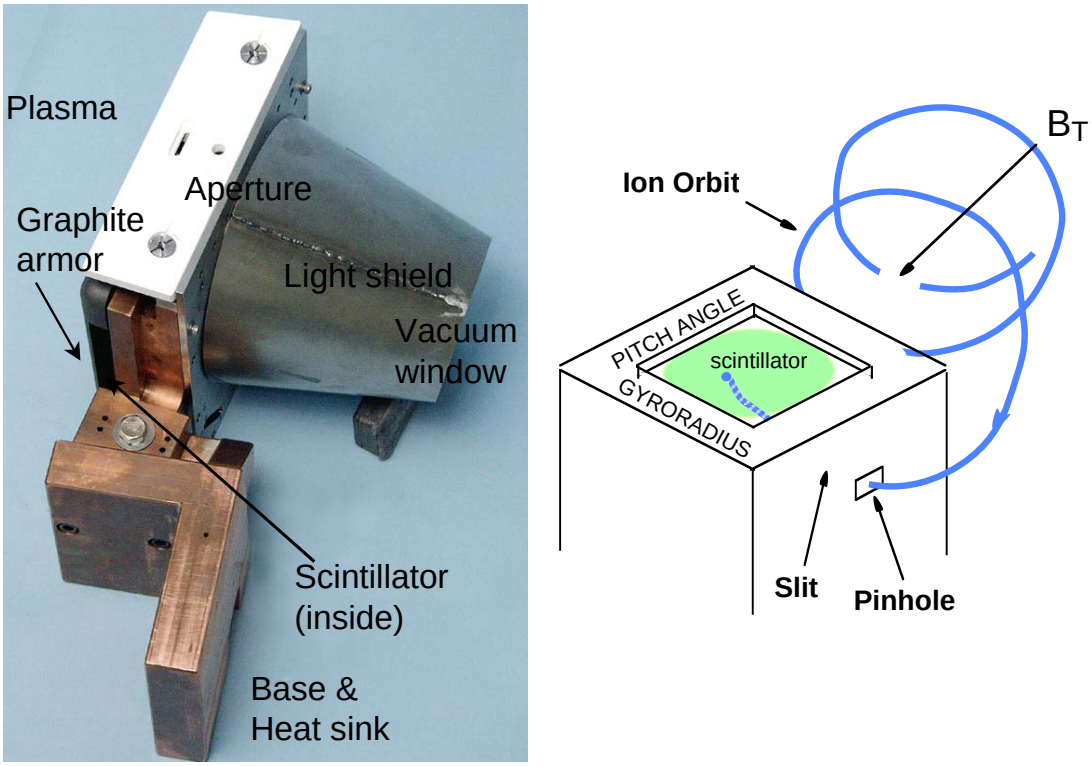

Fig. 2.21 NSTX fast lost-ion probe

2.2.3.3 Turbulence Diagnostics

Tangential microwave scattering – To investigate the short wavelength turbulence thought to be responsible for the anomalous electron transport on NSTX, a system is being designed, in collaboration with UC Davis, to detect small-angle scattering from a tangential microwave probing beam at wavelength $\lambda \sim 1$ mm. With the assumption that the turbulent fluctuations satisfy $\mathbf{k} \bullet \mathbf{B} \sim 0$, ray-tracing analysis of the k-matching condition for the proposed launcher and detector geometry indicates that the scattering occurs in a region with a radial extent of ~ 4 cm near the tangency point. This good spatial localization is a feature of the ST geometry. Furthermore, high scattered signals are anticipated because of the large electron gyroradius in the low magnetic field. In the proposed design, scattered beams are collected at five discrete detection angles corresponding to a range of k_r where electron temperature gradient (ETG) driven modes are predicted on NSTX. A steerable collection mirror provides considerable flexibility in the choice of R and k_r. Fig. 2.22 shows the complexity of the vacuum interface for this diagnostic, which must coexist with several existing systems.

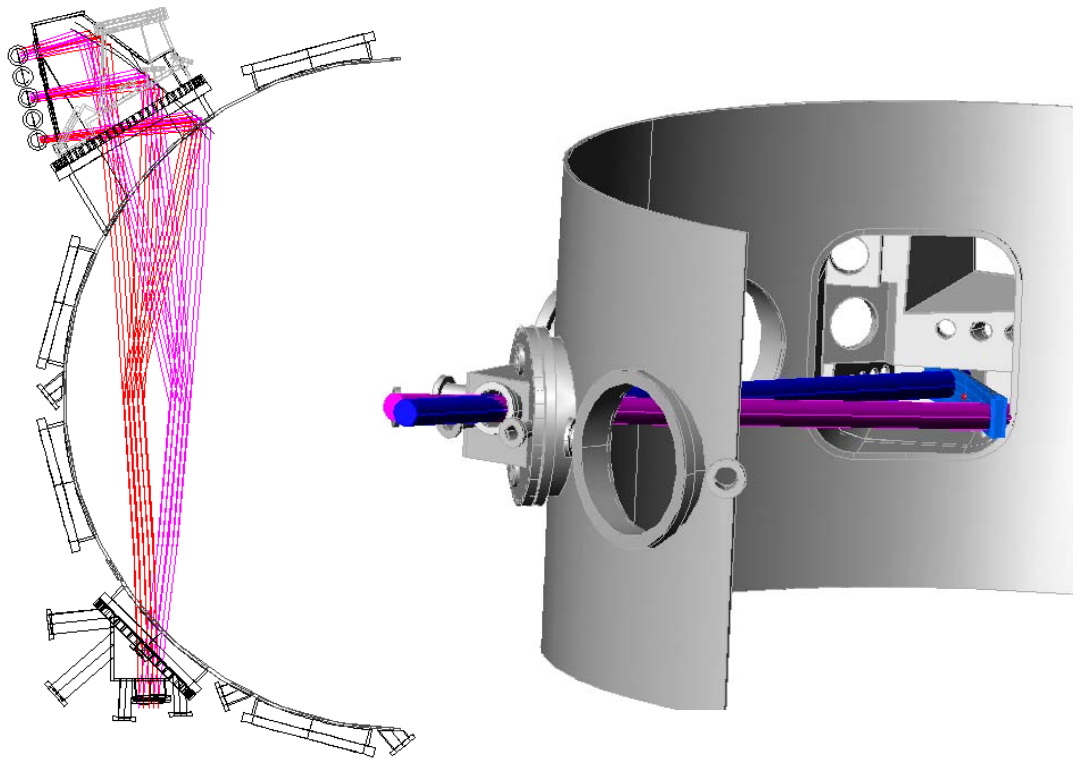

Fig. 2.22 Sightline and vacuum interface concept for tangential microwave scattering.

Microwave backscattering – Collaborators from UC Los Angeles propose in FY 04 to modify the existing port and antennae used for reflectometry to measure collective back-scattering at probe-beam frequency of ~100 GHz. This will also provide a method of detecting the existence of high-k ETG modes.

Imaging reflectometry for low-k core turbulence – NSTX is planning, over the next three years, to implement an imaging reflectometer, similar to that being developed for TEXTOR as a collaboration between FOM (Netherlands), UC Davis and PPPL As demonstrated recently by laboratory measurements, this new approach holds considerable promise for extending the applicability of reflectometer fluctuation measurements. One difficulty in implementing this diagnostic is the large optical access needed, although, on NSTX, the situation is ameliorated by the fact that the viewing window can be quite close (~ 40 cm) to the region of interest in the plasma. Fig. 2.23 shows the proposed optical design for this NSTX system.

Planar Laser Induced Fluorescence (PLIF) Visualization of Turbulence – Nova Photonics is developing, as a Phase II SBIR project, a diagnostic for visualizing edge turbulence in NSTX. A high-power laser (frequency-doubled alexandrite, 350 – 400 nm) will deliver a burst of 10 – 20 laser pulses within a single pump pulse, which lasts ~150 μs. The beam will be expanded to a planar sheet across the object plane of an ultra-fast CCD camera, filtered to record the laser-induced fluorescence at 488 nm from argon ions

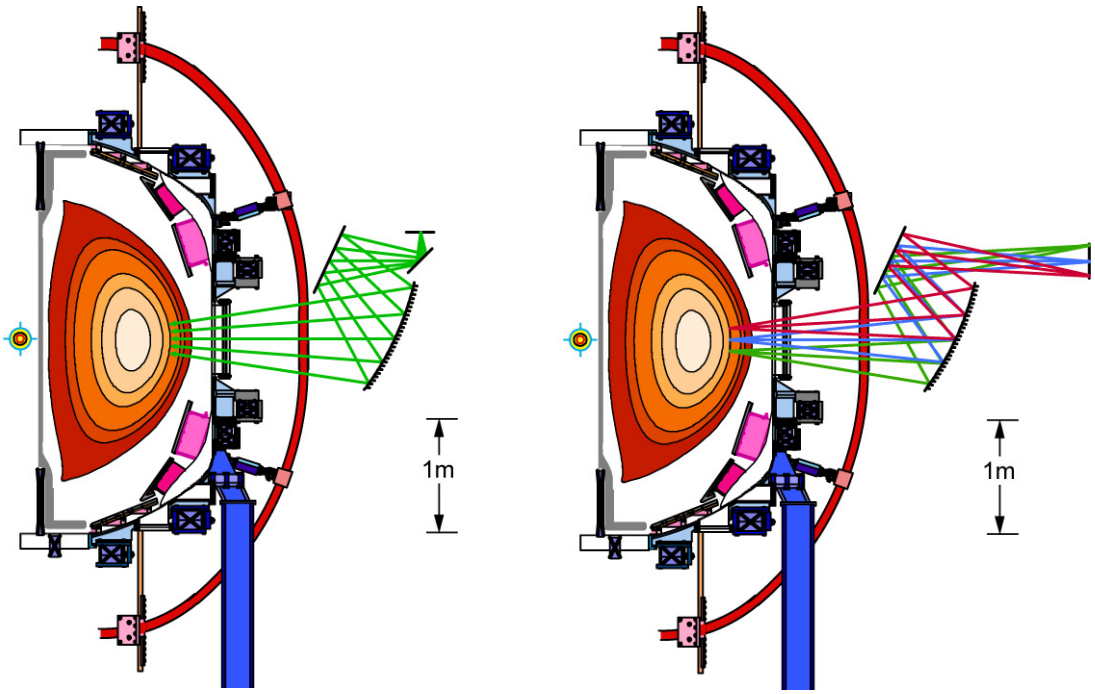

Fig. 2.23 Optical concept for imaging reflectometry illumination (left) and detection (right).

introduced into the plasma. This fluorescence will be proportional to the local argon-ion density, so the evolution of the turbulent density fluctuations can be followed. The camera, developed by Princeton Scientific Instruments, Inc., can record 28 images at a maximum rate of 1 MHz. It will be shared with the GPI diagnostic previously described.

2.2.3.4 Boundary Physics Diagnostics

Divertor bolometers – Currently a 4-channel foil bolometer is being evaluated for measuring radiated power in the NSTX divertor region. This system views from the outside radially in a vertical fan. If this evaluation is successful, this radial view will be upgraded to 16 channels, and a second 16-channel vertical view from the top of the machine will be added, also in a radial fan, to permit 2-D tomographic reconstruction of the radiated power from the divertor region.

Fast IR camera – NSTX currently employs two compact IR cameras with micro-bolometer array sensors. These cameras view directly through an IR window and their compact size allows for a modest amount of iron shielding. However, these cameras have a response time of about 50 ms which is too long to resolve many interesting surface temperature transients at the divertor strike points. An additional fast IR camera is planned with a response time of 30 – 50 μs for such studies, which will be carried out in collaboration with ORNL. It is likely that such a camera will be physically larger and therefore more difficult to shield at the viewing window, so a periscope would be needed to relay the image to a location compatible with shielding needs.

Line-filtered 1-D CCD cameras – NSTX currently employs two 1-D CCD cameras to view the D_α line emission from the divertor and edge. Additional cameras will be added in FY 04 and FY 05 to provide enhanced localization for the study of edge recycling.

Divertor spectroscopy – Other than a few sightlines with limited spatial resolution which are part of a visible survey spectrometer, NSTX has no spectroscopy for the divertor region. Two systems are planned to fill this gap. The first is a visible imaging spectrometer along with suitable fiber views of the divertor to study flows in this region. The second is a vacuum UV survey spectrometer (SPRED) similar to that currently employed at the midplane.

Edge Doppler spectroscopy upgrade – There is considerable interest in measuring detailed profiles of the ion temperature and flow velocity in the pedestal of H-mode plasmas. The prototype edge-rotation diagnostic, described in Sec. 2.1.4, has demonstrated that sufficient light can be gathered from the intrinsic carbon emission in this region to measure spectra on a very dense fan of sightlines through the edge with sufficient accuracy to perform an Abel inversion to obtain the radial profiles of the ion temperature and the plasma flow velocity in the pedestal. To accomplish this, smaller optical fibers would be substituted in the light collection system and a faster CCD detector would be used. Access for this diagnostic through the secondary passive plates will be maintained during the proposed relocation of the passive stabilizer plates described in Sec. 2.2.1.2.

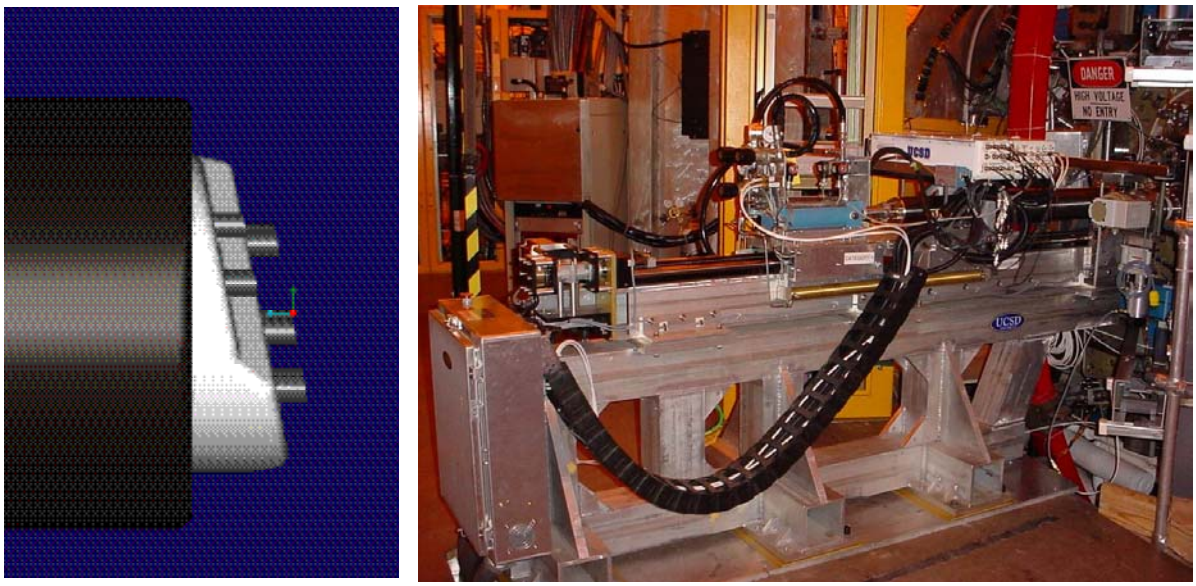

Fig. 2.24 NSTX fast reciprocating probe with contoured probe head

Midplane reciprocating probe – The fast reciprocating probe developed and installed by collaborators from UC San Diego will be upgraded in FY 04 with probe head featuring 10 tips positioned on a contour matching the flux surface geometry at its location ~17 cm below the midplane. A photo of the probe and model of the new contoured head are shown in Fig. 2.24. Two tips will be used as a double probe to measure T_e and n_e profiles. Other tips will be used to measure E_r and E_{pol} and fluctuations in these quantities. Additional upgrades being planned for this system include an interchangeable probe head with fast pickup coils to measure fluctuating magnetic fields. By measuring the fluctuations in both the local electric and magnetic fields, it would be possible to characterize the possible plasma dynamo action occurring during CHI.

Divertor fixed Langmuir probes – A number of tiles in the inner and outer divertor region are already equipped with a single flush-mount Langmuir probe. At present, 10 of these probes are instrumented and producing data, although reliable electrical isolation has been a problem. A higher density array of probes, with three or four probes per tile on several divertor tiles is planned. A domed design is being developed to better define the projected area.

Divertor fast reciprocating probe – A fast reciprocating probe for the lower divertor region is planned for deployment in the FY 06 – 07 period. This diagnostic would use one of the lower horizontal ports, providing access to the x-point region. Access through the new secondary passive plates for this and other divertor diagnostics will be part of the requirement for the proposed relocation of the passive stabilizer plates described in Sec. 2.2.1.2.

Deposition monitors – A sensitive deposition monitor has recently been installed on NSTX which measures the mass of the film deposited on a quartz crystal facing the plasma by detecting the change in its resonant frequency compared to that of a reference crystal which does not face the plasma. The measuring crystal was initially placed ~ 80 cm from the plasma edge and 33 cm below the midplane. An overall trend of deposition was recorded in a sequence of NSTX shots, punctuated by significant erosion on one shot which suffered a fast disruption. A second such monitor will be installed in FY 04, with the measuring crystal exposed to the divertor region through a gap in the outer divertor plate.

The composition of the material deposited at the vessel wall over the course of a run is currently obtained from the analysis of wall coupons which are removed when the vacuum vessel is opened. The surface layers of the coupons are analyzed using the standard techniques of Auger Electron Spectroscopy (AES), X-ray Photoelectron Spectroscopy (XPS) and Secondary Ion Mass Spectrometry (SIMS). Additional accelerator-based analysis of the composition has been performed by collaborators at Sandia National Laboratory. To supplement the data from the deposition monitors and wall coupons, a multi-purpose sample exposure probe, similar to the DIMES probe on DIII-D, is proposed for FY 07 to characterize the material deposited in the divertor region, time resolved through the course of the experiments, for the study of erosion and redeposition processes.

Helium jet spectroscopy – This diagnostic will consist of a gas nozzle mounted on the outboard mid-plane to inject a collimated beam of helium gas into the edge and a high resolution spectroscopic imaging system for the neutral helium emission. The measurements will provide the temperatures, densities and flow in the plasma edge and scrape off for comparison with models of edge transport and turbulence.

Divertor Thomson scattering – The large vertical ports in the lower dome of the NSTX vacuum vessel offer favorable access opportunities for a Thomson scattering measurement in the lower divertor region, based on the proven combination of a Nd-YAG laser with interference-filter polychromators and APD detectors, optimized for the lower temperatures expected in this region.. The observation sightlines for this measurement will pass through the secondary passive plates which will be modified during their relocation, discussed in Sec. 2.2.1.2.

Energy extract analyzer – It is proposed to measure the ion parallel and perpendicular temperatures in the divertor with a gridded ion energy analyzer. The grid has a programmable retarding potential and is used as an energy discriminator; a microchannel plate serves as a charge multiplier. The parallel thermal and drift velocities are obtained from the dependence of the collector signal on the retarding potential, and the perpendicular temperature is obtained from the ratio of currents to two sides of the detector.

References for Chapter 2

Facility and Initial Operations Overview Papers:

C. Neumeyer, *et al., Engineering Overview of the National Spherical Torus Experiment,* Proceedings of 17th Symposium on Fusion Engineering, San Diego, CA, October 1997, p. 238.

C. Neumeyer, *et al.*, *NSTX Construction, Commissioning and Initial Operations*, Proceedings of 18th Symposium on Fusion Engineering, October 1999, Albuquerque, NM, p. 63.

M. Ono, *et al.*, *Making of the NSTX Facility*, Proceedings of 18th Symposium on Fusion Engineering, October 1999, Albuquerque, NM, p. 53.

M. Ono, *et al.*, *Exploration of Spherical Torus Physics in the NSTX Device*, Nucl. Fusion **40**, 557 (2000).

C. Neumeyer, *et al.*, *Engineering Design of the National Spherical Torus Experiment*, Fusion Engineering and Design, Volume 54, Issue 52, January 2001.

C. Neumeyer, *et al.*, *National Spherical Torus Experiment Engineering Overview and Research Results 1999-2000,* Proceedings of 21st Symposium on Fusion Technology, Madrid, Spain, September 2000.

C. Neumeyer, *et al.*, *National Spherical Torus Experiment Engineering Overview and Research Results 1999-2000,* Fusion Technology, Volume 39, March 2001, p. 469.

M. Ono, *et al.*, *Overview of the Initial NSTX Experimental Results,* Nucl. Fusion **41**, 1435 (2001).

Vacuum Vessel and Coil System Related Papers

J. Chrzanowski, J. Spitzer, J. Citrolo, A. Brooks, H.M. Fan, C. Neumeyer, P. Heitzenroeder, and the NSTX Team, *NSTX Center Stack Design and Assembly*, Proceedings of 17th Symposium on Fusion Engineering, San Diego, Ca, October 1997, p. 637.

J. Chrzanowski, *et al.*, *NSTX Torus Design, Fabrication and Assembly,* Proceedings of 18th Symposium on Fusion Engineering, October 1999, Albuquerque, NM, p. 59.

P. Goranson, *et al.*, *Design of the Plasma Facing Components for NSTX*, Proceedings of 18th Symposium on Fusion Engineering, October 1999, Albuquerque, NM, p. 59.

C. Neumeyer, *et al.*, *Spherical Torus Center Stack Design*, Proceedings of 19th Symposium on Fusion Engineering, Atlantic City, New Jersey, January 2002.

Power System Related Papers

S. Ramakrishnan, *et al.*, *NSTX Electrical Power Systems,* Proceedings of 18th Symposium on Fusion Engineering, October 1999, Albuquerque, NM, p. 281.

Central Instrumentation and Control Related Paper:

C. Neumeyer, *et al., Real Time Control System of the National Spherical Torus Experiment*, IEEE Conference on Real Time Control, Santa Fe, New Mexico, June 1999

C. Neumeyer, *et al.*, *NSTX Power Supply Real Time Controller,* Proceedings of 18th Symposium on Fusion Engineering, October 1999, Albuquerque, NM, p. 285.

P. Sichta, *et al.*, *Startup of the Experimental Physics Industrial Control System (EPICS) at NSTX,* Proceedings of 18th Symposium on Fusion Engineering, October 1999, Albuquerque, NM, p. 289.

P. Sichta, *et al.*, *The NSTX Central Instrumentation and Control System,* Proceedings of 18th Symposium on Fusion Engineering, October 1999, Albuquerque, NM, p. 292.

D. Mastrovito, *et al.*, *Residual Gas Analyzer Hardware and Software Data Acquisition System at NSTX,* Proceedings of 19th Symposium on Fusion Engineering, Atlantic City, NJ, January 2002, p. 234.

P. Roney, *et al.*, *Computer and Network Infrastructure of the NSTX,* Proceedings of 19th Symposium on Fusion Engineering, Atlantic City, NJ, January 2002, p. 238.

S. Sengupta, *et al.*, *The NSTX Trouble Reporting System,* Proceedings of 19th Symposium on Fusion Engineering, Atlantic City, NJ, January 2002, p. 242.

P. Sichta, *et al.*, *Status of the Experimental Physics and Industrial Control System (EPICS) at NSTX,* Proceedings of 19th Symposium on Fusion Engineering, Atlantic City, NJ, January 2002, p. 245.

R. Marsala, H. Schneider, *NSTX Real Time Plasma Control Data Acquisition Hardware*, Proceedings of 22nd Symposium on Fusion Technology, Helsinki, Finland, September 2002.

Auxiliary Systems

L. Dudek, *et al.*, *Design and Construction of the NSTX Bakeout, Cooling, and Vacuum Systems,* Proceedings of 18th Symposium on Fusion Engineering, October 1999, Albuquerque, NM, p. 277.

H. Kugel, *et al.*, *NSTX Filament Preionization and Glow Discharge Cleaning Systems,* Proceedings of 18th Symposium on Fusion Engineering, October 1999, Albuquerque, NM, p. 296.

M. Kalish, *et al.*, *Design of the NSTX Heating and Cooling System,* Proceedings of 19th Symposium on Fusion Engineering, Atlantic City, NJ, January 2002, p. 230.

W. Blanchard, *et al.*, *Boronization on NSTX using Deuterated Trimethylboron,* Proceedings of 19th Symposium on Fusion Engineering, Atlantic City, NJ, January 2002, p. 226.

Diagnostic Systems

H. Kugel, *et al.*, *NSTX High Temperature Sensor Systems,* Proceedings of 18th Symposium on Fusion Engineering, October 1999, Albuquerque, NM, p. 300.

B. McCormack, *et al.*, *Rogowski Loop Designs for NSTX*, Proceedings of 18th Symposium on Fusion Engineering, October 1999, Albuquerque, NM, p. 306.

R. Parsells, *et al.*, *Multipulse Thomson Scattering System for NSTX,* Proceedings of 18th Symposium on Fusion Engineering, October 1999, Albuquerque, NM, p. 310.

R. Kaita, *et al.*, *NSTX Diagnostics for Fusion Plasma Science Studies*, IEEE Transactions on Plasma Science **30**, 219-226 (2002).

D. Johnson and NSTX Team, *Diagnostic Development for ST Plasmas on NSTX*, Presented at German-Polish EURO-Conference on Plasma Diagnostics for Fusion and Applications, Greifswald, Germany, September 4-6, 2002.

M. Gilmore, *et al.*, *A Practical Magnetic Field Strength Diagnostic for Low-Field Fusion Plasmas Based On Dual Mode Correlation Reflectometry*, Rev. Sci. Instrum. **74**, 1469 (2003).

S. Kubota, *et al.*, *Automatic Profile Reconstruction for Millimeter Wave FM-CW Reflectometry on NSTX*, Rev. Sci. Instrum. **74**, 1477 (2003).

K.C. Lee, *et al.*, *A Stark-tuned Laser Application for Interferometry and Polarimetry on the National Spherical Torus Experiment*, Rev. Sci. Instrum. **74**, 1621 (2003).

B.H. Deng, *et al.*, *Development of a Multichannel Far Infrared Tangential Interferometer/Polarimeter for the National Spherical Torus Experiment*, Rev. Sci. Instrum. **74**, 1617 (2003).

X. Zhang, *et al.*, *Trajectory Simulations for an NSTX HIPB*, Rev. Sci. Instrum. **74**, 1842 (2003).

S. Medley, *et al.*, *Initial Neutral Particle Analyzer Measurements of Ion Temperature on NSTX*, Rev. Sci. Instrum. **74**, 1896 (2003).

R. Raman, *et al.*, *Fast Neutral Pressure Measurements on NSTX*, Rev. Sci. Instrum. **74**, 1900 (2003).

A. Alekseyev, *et al.*, *Application of Natural Diamond Detector to Energetic Neutral Particle Measurements on NSTX*, Rev. Sci. Instrum. **74**, 1905 (2003).

P. Beiersdorfer, *et al.*, *High Resolution Soft X-ray Spectrometer for NSTX*, Rev. Sci. Instrum. **74**, 1974 (2003).

M. Bitter, *et al.*, *Results from the NSTX X-ray Crystal Spectrometer*, Rev. Sci. Instrum. **74**, 1977 (2003).

D. Stutman, *et al.*, *Integrated Impurity Diagnostic Package for Magnetic Fusion Experiments*, Rev. Sci. Instrum. **74**, 1982 (2003).

H. Blagojevic, *et al.*, *Imaging Transmission Grating Spectrometer for Magnetic Fusion Experiments*, Rev. Sci. Instrum. **74**, 1988 (2003).

R. Maqueda, *et al.*, *Gas Puff Imaging of Edge Fluctuations on NSTX*, Rev. Sci. Instrum. **74**, 2020 (2003).

V. Soukhanovskii, *et al.*, *High Resolution Spectroscopic Diagnostic for Divertor and Scrape-off Layer Neutral and Impurity Profile Measurements in NSTX*, Rev. Sci. Instrum. **74**, 2094 (2003).

D. Pacella, *et al.*, *Fast X-ray Imaging of the NSTX Plasma with a Micro Pattern Gas Detector based on GEM Amplifier*, Rev. Sci. Instrum. **74**, 2148 (2003).